Journal of Medicinal Chemistry

Article

Structure-Based Design and Optimization of Multitarget-Directed 2*H*-Chromen-2-one Derivatives as Potent Inhibitors of Monoamine Oxidase B and Cholinesterases

Roberta Farina, Leonardo Pisani, Marco Catto, Orazio Nicolotti, Domenico Gadaleta, Nunzio Denora, Ramón Soto-Otero, Estefanía Méndez-Álvarez, Carolina S. Passos, Giovanni Muncipinto, Cosimo D. Altomare, Alessandra Nurisso, Pierre Alain Carrupt, and Angelo Carotti

J. Med. Chem., **Just Accepted Manuscript** • Publication Date (Web): 24 Jun 2015

Structure-Based Design and Optimization of Multitarget-Directed 2*H*-Chromen-2-one Derivatives as Potent Inhibitors of Monoamine Oxidase B and Cholinesterases.

Roberta Farina,[a] Leonardo Pisani,[a] Marco Catto,[a] Orazio Nicolotti,[a] Domenico Gadaleta,[a] Nunzio Denora,[a] Ramon Soto-Otero,[b] Estefania Mendez-Alvarez,[b] Carolina S. Passos,[c] Giovanni Muncipinto,[a,†] Cosimo D. Altomare,[a] Alessandra Nurisso,[c] Pierre-Alain Carrupt,[c] Angelo Carotti*[a]*

[a] Dipartimento di Farmacia − Scienze del Farmaco, Università degli Studi di Bari "Aldo Moro", Via E. Orabona, 4, I-70125 Bari, Italy

[b] Grupo de Neuroquimica, Departamento de Bioquimica y Biologia Molecular, Facultad de Medicina, Universidad de Santiago de Compostela, San Francisco I, E-15782, Santiago de Compostela, Spain

[c] School of Pharmaceutical Sciences, University of Geneva, University of Lausanne, Quai Ernest Ansermet, 30, CH-1211, Geneva 4, Switzerland

KEYWORDS: monoamine oxidase inhibitors; acetylcholinesterase inhibitors; multi-target ligand design; Alzheimer's disease; Parkinson's disease; neurodegenerative diseases; coumarin derivatives.

ABSTRACT

The multifactorial nature of Alzheimer's disease calls for the development of multitarget agents addressing key pathogenic processes. To this end, by following a docking-assisted hybridization strategy, a number of aminocoumarins were designed, prepared and tested as monoamine oxidases (MAOs), acetyl- and butyryl-cholinesterase (AChE and BChE) inhibitors. Highly flexible *N*-benzyl-*N*-alkyloxy coumarins **2-12** showed good inhibitory activities at MAO-B, AChE and BChE, but low selectivity. More rigid inhibitors, bearing *meta*- and *para*-xylyl linkers, displayed good inhibitory activities and high MAO-B selectivity. Compounds **21**, **24**, **31**, **37** and **39**, the last two featuring an improved hydrophilic/lipophilic balance, exhibited excellent activity profiles with nanomolar inhibitory potency toward hMAO-B, high hMAO-B over hMAO-A selectivity and sub-micromolar potency at hAChE. Cell-based assays of BBB-permeation, neurotoxicity and neuroprotection supported the potential of compound **37** as a BBB-permeant neuroprotective agent against H_2O_2-induced oxidative stress with poor interaction as P-gp substrate and very low cytotoxicity.

INTRODUCTION

Neurodegenerative diseases (NDs) are widely investigated pathologies, because of the low efficacy of current therapies[1,2] and severe functional impairments for daily life activities resulting in high familiar, social and financial costs of patient care.[3] Despite the huge efforts in private and public research settings, most clinical trials of potential drug candidates for NDs, and for

Alzheimer's disease (AD) in particular,[4,5] failed. As a result, valuable disease-modifying therapies for NDs are still missing.

AD and Parkinson's disease (PD) are the most widespread and severe NDs. AD is the result of a progressive loss of neurons in basal forebrain regions, associated to abnormal accumulation of beta amyloid protein (Aβ) in neuronal plaques and hyper-phosphorylated tau protein in neurofibrillary tangles.[6] Neuronal degeneration in AD is triggered and maintained by low molecular weight Aβ oligomers and by reactive oxygen species (ROS), produced by oxidative degradation of neurotransmitters and xenobiotics.[7] The brain regions mostly affected by neuronal loss are essentially made of cholinergic neurons, so that restoring physiological acetylcholine levels has been considered a viable therapy in AD, as claimed by the so-called *cholinergic hypothesis*.[8] To date, drugs approved for AD therapy are the cholinesterase (ChE) inhibitors rivastigmine, galantamine and donepezil[9,10] (Chart 1). The NMDA partial antagonist memantine has also been approved for the symptomatic treatment of AD for its contrasting effects over glutamate excitotoxicity.[11]

Acetylcholinesterase (AChE, EC 3.1.1.7), the key enzyme targeted in the palliative therapy of AD, is present in both central and peripheral nervous system and in muscular motor plaques, and is responsible for the enzymatic cleavage of neurotransmitter acetylcholine (ACh). The other ChE, butyrylcholinesterase (BChE, EC 3.1.1.8), present in brain and peripheral tissues, but prevalently in serum, is up-regulated in advanced AD and may play a role in the maintenance and progression of the disease.[12]

The catalytic cleavage of ACh involves a tight cooperation of three amino acids, the so-called catalytic triad (Ser-His-Glu) and aromatic amino acid residues responsible for cation-π interactions.[13] The catalytic bottom cleft represents one of the binding sites for substrates and

inhibitors, along with the peripheral anionic binding site constituted by a larger region lined chiefly by aromatic amino acids. This structural arrangement accounts for the strong binding interactions observed for inhibitors such as decamethonium and donepezil, able to interact with both catalytic (CAS) and peripheral (PAS) anionic binding sites of AChE and, therefore, called dual binding site (DBS) inhibitors.[14] As binding interactions at the PAS reduces the aggregation of Aβ peptide(s) leading to amyloid oligomers DBS inhibitors are endowed with dual inhibitory activity on AChE and Aβ aggregation.[15]

The availability of X-ray crystallographic coordinates of many AChE-inhibitor complexes has allowed the identification of key interactions for high ligand binding affinity[16] and has enabled the target-based design of potent and selective AChE inhibitors (AChEIs). In this context, potent AChE inhibition by coumarin derivatives,[17,18] homo- and hetero-bis-quaternary ammonium salts,[19,20] 2-quinolones[21] and other heterocyclic compounds[22-24] have been reported by our group.

In the therapy of PD, a key target enzyme is represented by monoamine oxidase (MAO; amine-oxygen oxidoreductase; EC 1.4.3.4), a FAD-dependent enzyme, responsible for oxidative deamination of amine neurotransmitters, including dopamine that is depleted in PD, and exogenous amines.[25,26] Two isoforms of MAO, namely MAO-A and MAO-B, have been characterized in terms of amino acid sequence, tissue distribution, and selectivity towards substrates and inhibitors.[27,28] Selective MAO-A inhibitors (MAO-AIs: e.g., clorgyline and moclobemide) are used in the treatment of depression, while selective MAO-BIs, i.e., rasagiline and selegiline, are employed as adjuvant or alternative drugs to L-DOPA in PD therapy.[29,30]

The resolution of the X-ray crystal structures of both human MAO-A[31,32] and MAO-B[33-35] bound to several inhibitors has newly spurred the research in the field of MAO inhibition, given

to its therapeutic potential in neurological disorders, including AD where selective MAO-BIs may play a role.[29,36]

Growing evidence in the last few years has outlined the multifactorial etiopathogenesis of AD, PD and other NDs. Actually, neurodegeneration is a complex pathological event resulting from the imbalance and deregulation of multiple biochemical pathways, ultimately depending on transcriptional and epigenetic modulations and on environmental factors.[37] As a consequence, holistic, multifaceted pathologies are currently tackled by a polypharmacological approach based on multi-targeted therapy.[29,38,39] The paradigm "one drug-one target" has nowadays evolved into a more challenging "one drug-more targets" approach, provided that a good balance among potencies and efficacy towards selected targets, and optimal ADME-T properties, can be achieved.[40-42]

MULTITARGET-LIGAND DESIGN: RATIONALE AND METHODS

The experience achieved by our group in the field of ligand- and target-based design of potent, selective and reversible MAO[43-50] and ChE inhibitors,[17-24] prompted us to further explore the challenging field of multi-targeted ligand design, by addressing compounds with dual MAO and AChE inhibition. The earliest application of this approach by us was reported nearly 15 years ago, when we discovered coumarin derivatives endowed with good and moderate inhibition against MAO-B and AChE, respectively.[51] Additional data have been later presented in an international meeting.[52]

Since then, many authors have described the potential therapeutic application of multimodal MAO-Is displaying additional activities, such as AChE inhibition,[53-59] metal ion chelation,[60]

antioxidant[61,62] and neuroprotective activities.[63] Further studies suggested the combination of MAO and ChE inhibition in the same molecule as a promising strategy in the treatment of AD.[64]

Starting from our previous findings[51] we designed, synthesized and tested a new series of suitably substituted coumarin derivatives with the aim of discovering multipotent compounds with different bioactivity profiles towards MAO-B and AChE. While MAO-B selectivity was an important goal of our study to avoid unwanted side effects arising from the intestinal MAO-A inhibition and the consequent hypertensive effect coming from tyramine-rich food (tyramine is indeed metabolized by intestinal MAO-A),[65] the lack of AChE over BChE selectivity was not deemed as important [66] due to a likely pathogenic role of BChE in advanced AD.[67]

The molecular framework of our new multi-target ligands was built following a hybridization strategy. Starting from known ligands of the two enzymes, simple pharmacophore motifs were selected and joined in a unique molecular entity. As molecular flexibility plays a key role in accommodating ligands inside the AChE narrow gorge, a small series of hybrids was designed by connecting the coumarin core of 7-(3-chlorobenzyloxy)-3-methylcoumarin (MC 1095)[45] to the *N*-benzylaminomethyl group characterizing many AChE inhibitors (e.g., donepezil) through a flexible spacer (Figure 1). The 2*H*-chromen-2-one ring of such compound was chosen as the moiety able to efficiently fit the MAO-B enzymatic cleft by facing the isoalloxazine ring of FAD. In the additional series of more rigid hybrids, to improve AChE inhibitory potency of 7-benzyloxycoumarins[44] we approached a "designing in" strategy[29,39,42] by adding in a suitable position of the coumarin ring a protonatable basic moiety that might bind CAS through π-cation interactions (Figure 2). Taking into account that, as recently reported,[68,69] the steric hindrance of substituents placed at position 4 of the coumarin ring exerts a negative impact on MAO affinity, the basic head was anchored to the 7-benzyloxy substituent. This rational hybrid design was

supported by prospective docking studies based on X-ray crystal structures of the two target enzymes. As suggested by docking calculations, the protonatable head may establish π-cation interactions at the CAS of AChE, while the coumarin moiety may interact with PAS.[17] Such a pose resembled that of donepezil in the PDB complexes (entries: 1EVE and 4EY7). As for the binding to MAO-B, docking studies revealed that the coumarin nucleus can be accommodated in the catalytic region in proximity of FAD thus matching the pose experimentally observed in the X-ray crystal structure of MAO-B selective coumarin inhibitor NW-1772 (Chart 1).[49] The spacer tethering the two main pharmacophore features, namely the coumarin nucleus and the protonatable amine moiety, was examined also in terms of a reduced flexibility, by synthesizing the *meta*- and *para*-xylyl derivatives listed in Table 2, to determine the optimal distance between the two key binding moieties in both target enzymes.

Docking studies suggested that both polymethylene and xylyl linkers overlaid, at least in part, with the 7-benzyloxy group of NW-1772 that faces the MAO-B entrance cavity (acting as B/A structural determinants for selectivity) and keeps the basic moiety close to the aromatic region more proximal to the solvent.

The newly synthesized coumarin derivatives **2**-**40**, **42**, **43** were tested in vitro for their inhibition of rat MAO-A and MAO-B (rMAOs), electric eel AChE (eeAChE) and equine serum BChE (esBChE). The quinolone isoster **45** was also synthesized and tested, taking into account our previous findings on AChE inhibitors,[21] with the aim of retaining activity towards the target enzymes, while possibly improving the pharmacokinetics properties (i.e., lowering lipophilicity and increasing metabolic stability). The most potent inhibitors at rMAO-B and eeAChE were also assayed on the human isoforms of the two MAOs and ChEs. The inhibition data of non-human and human enzymes are reported in Tables 1-3 and 4, respectively. Finally, compound

37, that showed outstanding activities on human enzymes together with well-balanced solubility/lipophilicity properties, was also investigated as potential CNS-permeant neuroprotective agent in vitro.

CHEMISTRY

Compounds **2-40** were prepared from bromo-coumarin intermediates **1a-k** through microwave-assisted reaction with appropriate benzylamines, in the presence of anhydrous potassium carbonate and a catalytic amount of potassium iodide, in anhydrous acetonitrile. Bromides **1a-k** were, in turn, prepared from 7-hydroxycoumarin derivatives and commercial dibromides, as depicted in Scheme 1. Synthesis of analogs **42** and **43** (Scheme 2) started from the reduction of 4-(bromomethyl)phenylacetic acid with $BH_3 \cdot SMe_2$ complex to obtain alcohol **41a** that was then coupled with 7-hydroxycoumarin. CBr_4/PPh_3-mediated bromination of **41b** afforded **41c** that underwent a final microwave-assisted nucleophilic substitution with the appropriate benzylamine yielding the desired coumarins **42-43**. As illustrated in Scheme 3, 7-hydroxy-2-quinolone **44b** was prepared from the condensation of *trans*-cinnamic acid chloride with *m*-anisidine followed by an intramolecular Friedel-Crafts acylation/dearylation[70] reaction in refluxing chlorobenzene in the presence of aluminum chloride as Lewis acid. Sequential regioselective alkylation of phenolic-OH with α,α'-dibromo-*p*-xylene and reaction of intermediate **44c** with benzylmethylamine in the usual conditions gave final compound **45**.

Analytical and spectroscopic data of tested compounds **2-40**, **42**, **43**, **45** are reported in Table 6 and Supporting Information.

BIOLOGICAL ASSAYS

All compounds were tested for their inhibitory activities on rat MAOs (rMAOs), electric eel AChE (eeAChE) and equine serum BChE (esBChE) enzymes. For MAO inhibition test, the protocol using mitochondrial rMAO-A and -B obtained from rat brain homogenates was used as previously described.[45] As for eeAChE and esBChE, the well-known Ellman's spectrophotometric test[71] was used to determine both IC_{50}s and inhibition kinetics. Results are reported in Tables 1-3 as IC_{50} (μM) or, for poorly active compounds, as percentage of inhibition at 10 μM. Inhibition kinetics plots are depicted in Figure 3.

Compounds **2**, **4**, **5**, **11**, **12**, **21**-**24**, **29**, **31**-**34**, **37**, **39**, **40** and **45** were also tested on human isoenzymes of MAOs (hMAOs) and/or ChEs (hChEs). While hChEs were tested through the Ellman's method, the assays for hMAOs were carried out with a fluorescence-based method using kynuramine as a non-selective substrate of hMAO-A and hMAO-B.[72] Results of inhibition tests on hMAOs and hChEs are reported in Table 4.

Apical to basolateral (AP-BL) and basolateral to apical (BL-AP) apparent permeability (P_{app}) of compound **37** was measured using Madin-Darby Canine Kidney (MDCK) cells, retrovirally transfected with the human MDR1 cDNA (MDCKII-MDR1). P_{app} and efflux ratio (ER) were calculated and reported in Table 5.

Cytotoxicity of compound **37** was evaluated in human neuroblastoma cell line SH-SY5Y through the 3-(4,5-dimethylthiazol-2-yl)-2,5-diphenyl-tetrazolium bromide (MTT) viability assay (Figure 8).[73] The same cell-based method was used to for preliminarily investigate the cytoprotective effects of compound **37** against cell death induced by H_2O_2 (Figure 9).

RESULTS AND DISCUSSION

For the sake of clarity, structure-activity and structure-selectivity relationships (SAR and SSR, respectively) will be discussed first separately for the different classes of compounds reported in Tables 1-3, then a comparison will be made among the inhibition data from rMAOs and eeAChE with the corresponding data from hMAOs, hAChE and to a lesser extent hBChE (Table 4).

SARs and SSRs of N-benzyl-N-alkyloxy coumarin derivatives (Table 1)

Compounds **2-12** were designed to investigate the effects on inhibition potency and selectivity at the target enzymes of the length of the polymethylene linker and of the *N*-substitution at the NH-benzyl moiety with methyl and ethyl groups. A few substituents were also introduced on the benzyl ring of compound **6**, bearing a pentamethylene linker, to extend the knowledge of SARs and SSRs.

The inhibition data in Table 1 showed that, with a few exceptions, the designed compounds display from low- to sub-micromolar potencies against rMAO-B and eeAChE, whereas potencies against rMAO-A and esBChE were slightly lower. As the result, promising dual MAO-B and AChE inhibitors were discovered with limited MAO-B over MAO-A and AChE over BChE selectivity.

Interestingly, compounds **3**, **5**, **6** and **12**, characterized by linkers of different length, displayed sub-micromolar affinities at both rMAO-B and eeAChE with a limited selectivity over rMAO-A and esBChE, respectively. The gradual elongation of the linker in the *N*-Me derivative **2**, affording compounds **4**, **6** and **11** provided a consistent increase of potency towards eeAChE (from 1.3 μM of **2** to 0.095 μM of **11**) and esBChE (from 7.8 μM of **2** to 0.67 μM of **11**) whereas an opposite effect was observed with rMAO-B (from 0.33 μM of **2** to 1.7 μM of **11**). Therefore, in this series of compounds, the goal of optimizing both MAO-B and AChE activities

could not be achieved by varying the length of the linker. However, moving from the *N*-methyl derivative **11** to the *N*-ethyl homologue **12** good activities at the three target enzymes, rMAO-B, eeAChE and esBChE, were obtained but along with a very low MAO-B over MAO-A selectivity (SI = 3; SI is the selectivity index calculated as the ratio IC_{50} MAO-A/IC_{50} MAO-B). Compound **11** was endowed with the highest eeAChE inhibitory potency within the whole examined series (IC_{50} = 0.095 μM) and, surprisingly, the highest rMAO-A inhibitory potency (IC_{50} = 0.51 μM) leading to a reversal of rMAO selectivity (SI = 0.3). Kinetics of eeAChE inhibition resulted in a mixed-type mechanism, as expected from putative dual binding site inhibitors (Figure 3A), with K_i equal to 0.080 ± 0.002 μM.

Notably, compounds with the longest linker **11** and **12** displayed the highest inhibitory potency on rMAO-A (IC_{50} = 0.51 and 2.1 μM, respectively) and ChEs (IC_{50} = 0.095 and 0.32 μM, respectively, at AChE, and 0.67 and 0.49 μM, respectively, at BChE). No clear relationship emerged from the comparison of inhibition potency of *N*-methyl and *N*-ethyl derivatives.

The introduction in compound **6** of a cyano group in position *meta* and *para* (**7** and **9**, respectively) and of a chlorine at position *meta* (comp. **8**) did diminish the inhibitory potency towards all the tested enzymes except for compound **8** at both ChEs.

SARs and SSRs of meta- and para-N,N-dialkylaminomethyl-7-benzyloxycoumarin derivatives (Table 2).

Compounds **13**-**40** were designed to investigate the effects on inhibition potency and selectivity at the three target enzymes of the *N,N*-dialkylaminomethyl substituents at the *meta* and *para* positions of the 7-benzyloxy moiety and of substituents at position 3 and 4 of the coumarin ring, having in mind our previous findings,[68,69] which highlighted the steric

requirements for this region in binding MAO-B enzymatic cleft. A number of substituents were also introduced on the *N*-benzyl ring in R_4 to extend the study of SARs and SSRs.

It is worth to underline that all the examined compounds shared a *meta*- or *para*-xylyl linker joining the oxygen at position 7 of coumarin with the basic *N,N*-dialkylamino substituents. Both xylyl linkers have a lower conformational flexibility compared to the polymethylene linkers of compounds **2-12** and this might result in a higher (iso)enzyme selectivity. Indeed, this was the case for rMAOs, as most compounds achieved micromolar to sub-micromolar rMAO-B inhibitory potency whereas an inhibition lower than 20% at 10 μM was generally displayed at rMAO-A. The same effect on selectivity was not observed for the ChEs even though most compounds appeared slightly more AChE-selective. Inhibition potency on eeAChE reached the sub-micromolar level in eleven cases, the most potent inhibitor being compound **24** (IC_{50} = 0.10 μM), while on esBChE only six compounds exhibited a sub-micromolar activity, with compound **19** showing the highest potency (IC_{50} = 0.24 μM).

As the *N,N*-dimethylaminomethyl derivative **13**, the lead compound of the *meta*-xylyl series, showed very low inhibitory effect on rMAO-A and eeAChE (IC_{50} = 10 μM and 38% inhibition at 10 μM, respectively) and moderate activity on rMAO-B and esBChE (IC_{50} = 3.2 μM and 5.3 μM, respectively), its *N,N*-diethylamino **14** and *N*-methyl-*N*-benzylamino **15** congeners were synthesized. Improved potencies were definitely gained with compound **15** that showed an interesting profile of inhibition with low micromolar potencies rMAO-B, eeAChE and esBChE (IC_{50} = 2.0, 2.3 and 1.0 μM, respectively) and very weak activity at rMAO-A (8% inhibition at 10 μM). The introduction of cyano, methoxy and chloro substituents at the *meta* position of the phenyl ring of the *N*-benzylamino moiety, leading to compounds **16**, **17** and **18**, respectively,

resulted in lower inhibitory potencies on rMAO-B and eeAChE whereas a 3-fold increased inhibition was observed for the chloro derivative **18** on esBChE (IC_{50} = 0.31 μM vs. 1.0 μM).

The *para*-*N,N*-dimethylamino- and *N,N*-diethylamino-methyl derivatives **19** and **20** displayed lower activity against rMAO-A, similar activity against rMAO-B, and higher activity against esBChE when compared to the corresponding *meta*-substituted isomers **13** and **14**. Better results were obtained with the *para N*-methyl, *N*-benzylaminomethyl derivative **21** that achieved sub-micromolar potency towards rMAO-B and eeAChE (IC_{50} = 0.85 and 0.75 μM, respectively), and a significantly lower activity against rMAO-A and esBChE (7% at 10 μM and IC_{50} = 11 μM, respectively).

Methyl substituents were introduced at the positions 3 and 4 of the coumarin ring to give the monomethyl derivatives **22** and **23** and the dimethyl derivative **24**. Compared to the lead compound **21**, the rMAO-B activity decreased while a significant increase of the inhibitory potency on eeAChE (IC_{50} = 0.26, 0.18 and 0.10 μM) and esBChE (IC_{50} = 1.1, 1.0 and 0.69 μM) was observed for compounds **22**, **23** and **24**, respectively. It is worth noting that these very simple structural changes led to the most potent eeAChE inhibitors of the whole series of compounds and, even more interestingly, for compound **24** an impressive combination of high inhibitory activities towards rMAO-B, eeAChE and esBChE and high rMAO-B-selectivity was revealed (IC_{50} = 1.2, 0.10 and 0.69 μM at rMAO-B, eeAChE and esBChE, respectively, and 0% inhibition at 10 μM at rMAO-A). As for open chain derivative **11**, also compound **24** displayed mixed-mode kinetics for eeAChE inhibition, with K_i equal to 0.22 ± 0.03 μM (Figure 3B).

As done for lead compound **15**, the isomeric compound **21** was modified by introducing cyano, methoxy and chloro substituents at position *meta*, and the cyano group at position para as well, in the aromatic ring of the *N*-benzylamino moiety. *Meta*-substituted derivatives **25**-**27**

proved to be less potent inhibitors than the lead compound **21** on rMAO-B. *Meta*-chloro derivative **27** maintained, however, an attractive inhibition profile (12% inhibition at 10 μM at rMAO-A; IC_{50} = 2.7, 0.59 and 1.2 μM, at rMAO–B, eeAChE and esBChE, respectively). Therefore, compound **27** was slightly modified by introducing methyl substituents at the positions 3 and 4 to afford the monomethyl derivatives **28** and **29** and the dimethyl derivative **30**. Compared to **27**, rMAO-B, rMAO-A and esBChE activities considerably decreased, while the potency towards AChE was maintained, or even improved in particular for the 4-methylderivative **29** (IC_{50} = 0.12 vs. 0.59 μM). Compared to **21**, 4-cyanobenzylamino derivative **31** displayed lower activities towards rMAO-A, eeAChE and esBChE and a 3-fold increase of rMAO-B activity. The introduction in compound **31** of methyl substituents at the positions 3 and 4, to give the monomethyl derivatives **32** and **33**, and the dimethyl derivative **34**, generally diminished the activity on almost all enzymatic targets.

The final structural modifications of lead compound **21** were aimed at reducing molecular lipophilicity while maintaining good inhibitory activities on the target enzymes. One approach aimed at the modulation of the pK_b of the basic head, through the elongation of an arm of the linker that allowed a higher distance between the two electron withdrawing phenyl rings from the basic nitrogen, resulting in lower pK_b and logD. This structural modification increased the distance between the two key binding moieties of **21**, that is the coumarin ring and the *N*-benzyl group, giving rise to the more flexible *N*-benzyl, *N*-phenethyl analog **42** (Table 3). In addition, *N*-demethylated derivative **43** was synthesized to test the effect of having a more hydrophilic basic moiety endowed with HB-donor ability. Compared to compound **21**, the homologue **42** showed a similar activity towards eeAChE (IC_{50} = 0.85 vs. 0.75 μM) and rMAO-A (12% vs. 7%), a much higher activity at esBChE (IC_{50} = 0.52 vs. 11 μM), and a decreased activity at

rMAO-B (IC_{50} = 4.1 vs. 0.85 μM). To our surprise, the *N*-demethylated congener **43** reversed MAO-selectivity, being the activity on rMAO-A higher than on rMAO-B (IC_{50} = 1.7 μM and 45% inhibition at 10 μM, respectively). The inhibition potency on eeAChE worsened (IC_{50} = 4.7 vs. 0.85 μM), while conversely the potency against esBChE remained nearly unchanged (IC_{50} = 0.64 vs. 0.52 μM). An additional less lipophilic analog of **21**, namely **45** in Table 3, was prepared through bioisosteric replacement of the 2*H*-chromen-2-one with the 2-quinolone as successfully done in the past for a dual binding site AChE inhibitor.[21] Actually, the activity towards both cholinesterases improved (IC_{50} = 0.49 vs. 0.75 μM and 1.7 vs. 11 μM at eeAChE and esBChE, respectively) and the low activity on rMAO-A was maintained but, unexpectedly, the activity on rMAO-B dramatically decreased (29% inhibition at 10 μM vs. IC_{50} = 0.85 μM).

As the homologation of the basic head and the isosteric replacement yielded unsatisfying results, compound **21** was modified by introducing polar groups on the coumarin core. The insertion of a polar cyano group on the coumarin ring at position 3 (comp. **35**) was highly detrimental for rMAO-B activity (41% at 10 μM vs. IC_{50} = 0.85 μM) while a 3- and 2-fold potency increase was observed against eeAChE (IC_{50} = 0.20 vs. 0.75 μM) and esBChE (IC_{50} = 5.5 vs. 11 μM), respectively. Better results on rMAO-B but much worse toward both ChEs came from the introduction of a second polar substituent, a *para*-cyano group on the *N*-benzyl ring (comp. **36**).

Guided by docking simulations and a 3D-QSAR model recently developed from a large series of 4,7-disubstituted coumarins,[69] a different, more polar substituent, that is the hydroxymethyl group, was introduced at position 4 of the coumarin core. Very satisfactorily inhibitor **37** showed good inhibitory activities with the three target enzymes (IC_{50} = 0.41, 0.42 and 1.1 μM at rMAO-

B, eeAChE and esBChE, respectively) and no activity on rMAO-A (0% inhibition at 10 μM). As for compounds **11** and **24**, also **37** showed a mixed-type inhibition mode (Figure 3C), with a K_i equal to 0.10 ± 0.01 μM. The *N*-demethylated derivative of **37**, that is comp. **38**, was also prepared and tested. Its inhibitory potencies and selectivity profile (IC_{50} = 0.53, 0.44 and 0.57 μM at rMAO-B, eeAChE and esBChE, respectively and 19% inhibition at rMAO-A at 10 μM) were very good and compared well with those of the *N*-methyl analog.

As previous SAR/3D-QSAR[45] and current docking studies (data not shown) suggested favorable interactions of a halogen atom at the *meta* position of a benzyl ring at AChE and MAO-B binding sites, the *meta*-chloro derivative **39** was synthesized and tested. Its excellent inhibitory activities on the three target enzymes (IC_{50} = 0.24, 0.25 and 0.63 μM for rMAO-B, eeAChE and esBChE, respectively, and 0% inhibition toward rMAO-A at 10 μM) proved the goodness of our molecular design. Indeed, compound **39** attained the pursued combination of strong and well-balanced inhibitory potencies and an excellent rMAO-B over rMAO-A selectivity.

The introduction of a *para*-cyano substituent in the *N*-benzyl ring of **37** led to **40** which showed an exquisite rMAO-B activity and selectivity (rMAO-B: IC_{50} = 0.035 μM; rMAO-A: 0% inhibition at 10 μM), but also a dramatic drop of activity at eeAChE (IC_{50} = 6.3 μM) and esBChE (23% inhibition at 10 μM), indeed resulting as the most potent MAO-B inhibitor of the whole set of compounds herein investigated.

Inhibitory activities on human enzymes

The good biological profiles of many inhibitors towards MAO and ChE enzymes, prompted us to extend our inhibition assays to the corresponding human enzymes. On the basis of our

previous studies,[72] significant changes of inhibitory activities were expected for hMAOs (generally an improvement, especially at hMAO-B) whereas more limited differences were awaited for hAChE inhibition. However, to gain further support to these general predictions and select compounds with high activity on hMAO-B and hAChE, a prospective docking study was performed on the series of inhibitors listed in Table 4. Inhibition activities on human enzymes were not assessed for compounds exhibiting low potency against the corresponding rMAO and eeAChE enzymes.

Prospective docking simulations were carried out using GOLD Suite v5.2[74] on the X-ray crystal structures of AChE and MAO-B available from the PDB. For AChE studies, the X-ray crystal structures of *Torpedo californica* AChE (TcAChE) (PDB entry: 1EVE) and human recombinant AChE (hAChE) (PDB entry: 4EY7), both complexed with donepezil, were used. The careful inspection of the two crystal structures revealed that PAS and CAS binding sites of AChE are at about 18 Å distance (measured between the Cα carbon atoms of Trp86 and Trp286 of hAChE). Distances between the two putative binding moieties close to such a value, might ensure efficient interactions at both PAS and CAS. On this basis, we conceived predictive docking studies aimed at forecasting the optimal length of the polymethylene spacer joining the pharmacophore features ensuring strong AChE binding. In this respect, the *in silico* studies were focused on two compounds (**2** and **11** of Table 1) bridging the protonatable basic tail and the coumarin head with a short (trimethylene) or long (hexamethylene) linear linker, respectively. Interestingly, docking simulations returned similar poses for the two compounds, which were both able to engage steady π-π stacking interactions with the aromatic residues of Trp86 and Trp286. The compound bearing the longer linear linker showed a higher score (-106.2 kJ/mol for hAChE and -96.3 kJ/mol for TcAChE) compared to that bearing the shorter linker (score: -98.2

kJ/mol for hAChE and -88.6 kJ/mol for TcAChE). For clarity, a zoomed in view of top-scored solutions is shown in Figure 4. Compounds **2** and **11** actually proved effective in inhibiting AChE, in good agreement with the docking scores.

For MAO-B studies, the X-ray crystal structure of hMAO-B (PDB entry: 2V60) and a homology model for the rMAO-B were used. We performed a number of exploratory docking runs to assess whether the decoration of the well known 7-benzyloxycoumarin with a protonatable amino tail (mimicking the basic head of donepezil) could be suitable in biasing also MAO-B. To this end, we docked three probe compounds (**23**, **32**, and **33** in Table 2) into the binding site of MAO-B, and observed that the *ad-hoc* incorporated benzylamine fragment was located in a peripheral region surrounded by Tyr112, His115 (mutated to Tyr115 in rMAO-B) and Asn116. As shown in Figure 5, the residue at position 115 is critical in establishing π-π stacking interactions with the terminal benzyl ring of **32**, although the scores at hMAO-B were consistently higher than those at rMAO-B. These interspecies differences were even more pronounced in enzyme inhibition potency of **32**, showing two log units higher activity at hMAO-B compared to rMAO-B (IC_{50} = 0.017 vs. 1.7 μM). We hypothesized that such scoring and biological differences in hMAO-B and rMAO-B can rely on a likely greater strength of the π-π stacking interactions engaged by the imidazole ring of His115 compared to that of the phenyl ring of Tyr115.[75]

The potential benefit of introducing a cyano group at the *para* position of the benzylamine was also challenged by docking compounds **23** and **33**. Actually, we did not observe any appreciable difference in the scores; however, the presence of the cyano group increased the rMAO-B inhibition approximately of 10 folds (**23**, IC_{50} = 4.1 μM vs. **33**, IC_{50} = 0.41 μM). We tentatively explained this experimental result by visually inspecting the docking poses of **23** and

33. As shown in Figure 6, the cyano group could form HBs (even water-mediated) with Asn116 or Tyr112.

For the sake of completeness, additional modeling studies were conducted on **37**, one of the most potent multi-target inhibitors of the series. **37** was first docked into both hAChE and TcAChE to assess the binding interactions resulting from the substitution of an aliphatic linker with an aromatic one and of the 4-H atom with a more polar 4-hydroxymethyl group. Beyond hydrophobic interactions already described for inhibitors **2** and **11** bearing an aliphatic linker, inhibitor **37** was engaged in a π-π interaction involving the *para*-xylyl linker and the aromatic side chain of Tyr341 (hAChE numbering referred to PDB entry 4EY7).[17] In addition, a HB occurred between the 4-hydroxymethyl group and Ser293 of hAChE as shown in Figure 7A. The higher score of **37** towards hAChE (-109.38 kJ/mol) compared to **2** and **11** may be therefore ascribed to both π-π and HB interactions (Figure 7A).

As reported in previous studies,[68,69] the introduction of polar groups at position 4 of the coumarin scaffold improved physicochemical relevant properties (e.g., aqueous solubility and lipophilicity) while maintaining good MAO-B inhibitory potency and selectivity. Thus inhibitor **37** was docked also on hMAO-B resulting in a binding pose similar to that of **23**, **32** and **33** but with a higher score (-95.95 kJ/mol). Most likely the high hMAO-B inhibitory potency arose from the formation of multiple HBs between the hydroxyl group and structural water molecules[45,49,68] as illustrated in Figure 7B.

Inhibition data in Table 4 fulfilled our expectations and docking calculations. As far as the inhibitory activities on hMAO-B are concerned, a consistent increase of activity, from 2.5-fold for compound **2** up to 121-fold for **34**, was recorded whereas the activities on hMAO-A remained low or were slightly incremented, from 2.7-fold for compound **11** to 18-fold for compound **12**. As the result, the hMAO-B over hMAO-A selectivity strongly raised. Actually, the SIs measured for compounds **37**, **39** and **40** were 2210, 842 and 910, respectively. Since for many other inhibitors activities on hMAO-A remained very low, the IC_{50} values were not measured and the hMAO selectivity could not be exactly assessed. Nevertheless, taking into account the low percentage of inhibition of hMAO-A at 10 μM concentration, high hMAO-B over hMAO-A selectivity can be confidently foreseen also for inhibitors **21**, **31** and **32**.

It is worth noting that all the coumarin derivatives listed in Table 4 attained sub-micromolar inhibitory on hMAO-B. Coumarin derivatives **37** and **40**, bearing the 4-CH_2OH group, were the most potent inhibitors within the whole molecular series examined with IC_{50} values in the low nanomolar range (10 and 5.7 nM, respectively). Interestingly, some similarities and striking differences emerged by comparing inhibitory activities at rat and human MAO enzymes. For instance, 4-CH_2OH-bearing coumarin derivatives **37**, **39** and **40** resulted the most active MAO-B inhibitors at both the human and rat enzymes, with compound **40** showing the highest activities (IC_{50} = 0.0057 and 0.035 μM, respectively). Noteworthy, the inverted selectivity observed on rMAOs for compound **11**, bearing the longest polymethylene linker, was maintained also on hMAOs.

As anticipated in the introduction, the selective inhibition of either AChE or BChE was not a primary aim of our work. Nonetheless a number of representative compounds, that is **5**, **11**, **21**, **24**, **37** and **39**, were tested also on hBChE (Table 4). Despite an 89.4 % of amino acid sequence

identity, the human and equine enzymes displayed significant differences in the catalytic site and even more in the peripheral sequence. Notably, Gly277, Pro285, Phe398 in human mutated to Asp, Leu and Ile, respectively, in equine. The amino acid numbering refers to hBChE as reported in PDB. Therefore different inhibition potencies at the two enzymes may be expected and this was indeed observed for compounds **24**, **39**, **21** and **37** (46% and 14% at 10 μM and IC_{50} = 0.89 and 9.3 μM versus IC_{50} = 0.69, 0.63, 11 and 1.1 μM respectively). In contrast, compounds **5** and **11** displayed sub-micromolar inhibition potencies on hBChE close to the ones observed on esBChE.

Appealing inhibition profiles resulted for compounds **5**, **37** and **39**. The first displayed sub-micromolar potencies at all the four tested human enzymes, along with a significant, but limited, selectivity for hMAO-B (SI = 13.5) and no selectivity for either one of the two ChEs. The latter two showed high hMAO-B inhibitory potencies and selectivities (IC_{50} = 10 and 24 nM, and SI = 1580 and 542, respectively) and also a good hAChE inhibitory potency and selectivity (IC_{50} = 0.12 and 0.33 μM , and SI = 77.5 and >>30, respectively).

Taking into account inhibition potencies, selectivity data and physicochemical parameters, inhibitor **37** was selected for a preliminary evaluation of its ability to cross blood-brain barrier (BBB) and its cytotoxicity and cytoprotective properties.

BBB PERMEABILITY AND TOXICITY PROFILING OF COMPOUND **37**

MDCK-MDR1 cell lines are known to express P-glycoprotein (P-gp), which plays an important role in the efflux transport of drugs from brain to blood. Thus, we were particularly interested to see if compound **37** was able to permeate by passive diffusion the BBB and to

interact with P-gp as well. To this purpose, transport studies were performed on MDCKII-MDR1 cells which are characterized by high P-gp expression, and represent a well-established *in vitro* model mimicking the BBB.[76,77] Transport studies were conducted in both apical-to-basal (AP-BL) and basal-to-apical (BL-AP) directions and the results were reported in Table 5. Fluorescein isothiocyanate-dextran (FD4) and diazepam were used as paracellular and transcellular markers, respectively, of cell monolayers integrity and as internal controls to verify tight junction integrity during the assay; the results for controls were within the expected values. Both apparent permeabilities (AP-BL: $1.91 \cdot 10^{-5}$ cm·sec^{-1}; BL-AP: $3.38 \cdot 10^{-5}$ cm·sec^{-1}) were comparable with those of diazepam, thus supporting a good BBB penetration. The efflux ratio (ER) equal to 1.77 detected for compound **37** disclosed no significant differences in P_{app} values between AP-to-BL and BL-to-AP direction. Since a value of ER greater than 2 indicates that a test compound is likely to be a substrate for P-gp transport, the measured value suggested that compound should be able to permeate the monolayer without significant interactions with such efflux system.

The effects of compound **37** on the viability of human neuroblastoma cell line SH-SY5Y were studied, using donepezil as reference compound. As shown in Figure 8, compound **37**, like donepezil, was not cytotoxic at the tested concentrations ranging from 0.1 to 50 μM after 24, 48 and 72 h of incubation. The neuroprotective capacity of **37** against oxidative stress was also evaluated using the same cell line and hydrogen peroxide (H_2O_2) for the generation of exogenous free radicals. Cells were incubated with **37** at two non-toxic concentrations (1 and 10 μM) for 24 h; then, H_2O_2 (60 μM) was added and the cells maintained for further 24 h. Cell death was determined using the MTT assay. As shown in Figure 9, compound **37** at 10 μM concentration prevented the H_2O_2-induced cell death (ca. 25%) with a statistically significant effect ($P < 0.01$).

CONCLUSIONS

The most salient features emerging from the SARs and SSRs of the two classes of compounds examined in this paper can be summarized as follows. Highly flexible inhibitors of the *N*-benzyl, *N*-alkyloxy coumarin series in Table 1 showed good inhibitory activities at the target enzymes, when bearing a penta- or hexamethylene linkers, but low selectivity (see comps. **6**, **11** and **12** in Table 1). The inhibitors bearing a more rigid xylyl linker (Table 2), displayed good inhibitory potencies and high rMAO-B over rMAO-A selectivity ratios. Compound **21**, a more rigid analog of **6**, exhibited good activities and selectivity towards rMAO-B and eeAChE. *Meta*-chlorobenzyl analogs (i.e., **27**, **35** and **39**) showed an improved inhibition at eeAChE and esBChE but a worse inhibition at rMAO-B, whereas in contrast the *para*-cyanobenzyl analogues **31**, **33** and **36** showed better potencies toward rMAO-B and decreased potencies toward eeAChE. The more polar and hydrophilic 4-hydroxymethyl derivatives **37**-**39** displayed the most interesting activity profiles with low submicromolar activity at the three target enzymes rMAO-B, eeAChE and esBChE, and low or no activity at rMAO-A.

More interesting results came from the assays of selected inhibitors on human MAOs and AChE. In comparison with non-human enzymes, a significant increase of inhibitory activities was observed for hMAOs, more pronounced on hMAO-B, with a consequent increase of the selectivity index. More limited variations, generally a decrease of inhibitory potency, were instead observed with hAChE and hBChE. The most interesting inhibitors, e.g. **5**, **12**, **21**, and **37**-**39**, showed excellent activity profiles with low nanomolar inhibitory potency on hMAO-B, high MAO-B over MAO-A selectivity and sub-micromolar potency on hAChE. Kinetic inhibition data and docking studies on selected compounds suggested a mixed-type mechanism of inhibition and binding interactions at both the CAS and PAS of AChE. Therefore our compounds

do behave as dual binding site inhibitors and have the potential to block another pathological mechanism of AD, that is the AChE-promoted A-beta aggregation taking place at the PAS.[78,79]

Ultimately, our hybridization strategy proved successful in designing and optimizing novel coumarin-containing compounds targeting MAO-B and ChEs, two key enzymes involved in AD, PD and other neurodegenerative diseases, with well-balanced inhibition potencies. Activity, selectivity and physicochemical properties were improved compared to other ligands targeting the same enzymes described so far.[53-57] Moreover, toxicity, neuroprotection and transport data, as preliminarily assessed using cell-based models, suggested that the 4-hydroxymethyl coumarin derivative **37**, which resulted the most promising inhibitor, is devoid of significant neurotoxicity, shows moderate neuroprotective effects against H_2O_2-induced cell death, as well as a good BBB permeability profile with limited P-gp affinity.

In conclusion, some of the multipotent inhibitors reported herein, and compound **37** in particular, may be considered promising leads for further pre-clinical studies in cognitive and neurodegenerative disease models.

EXPERIMENTAL SECTION

Chemistry.

Starting materials, reagents, and analytical grade solvents were purchased from Sigma-Aldrich Europe. All reactions were routinely checked by TLC using Merck Kieselgel 60 F254 aluminum plates and visualized by UV light. Microwave reactions were performed in a Milestone MicroSynth apparatus, setting temperature and hold times, fixing maximum irradiation power to 500 W and heating ramp times to 2 minutes. The purity of all the intermediates was checked by ^{1}H NMR and ESI-MS. ESI-MS analyses were performed on an Agilent 1100 LC–MSD trap

system VL. Flash chromatographic separations were performed on a Biotage SP1 purification system using flash cartridges prepacked with KP-Sil 32−63 μm, 60 Å silica. Elemental analyses were performed on a EuroEA 3000 analyzer only on the final compounds and are reported in Supporting Information. The measured values for C, H, and N agreed to within ±0.40% of the theoretical values. Melting points (MP) were taken on a Gallenkamp MFB 595010M apparatus (open capillary method) and are uncorrected. Nuclear magnetic resonance (NMR) spectra were recorded at 300 MHz on a Varian Mercury 300 instrument at ambient temperature in the specified deuterated solvent. Chemical shifts (δ) are quoted in parts per million (ppm) and are referenced to the residual solvent peak. The coupling constants J are given in hertz (Hz). The following abbreviations were used: s (singlet), d (doublet), t (triplet), dd (doublet of doublet), m (multiplet), brs (broad signal). Signals due to NH/OH protons were located by deuterium exchange with D_2O. Non-commercial 7-hydroxy-3-methylcoumarin,[45] 7-hydroxy-3,4-dimethylcoumarin,[44] 7-hydroxy-3-cyanocoumarin,[80] 7-hydroxy-4-(hydroxymethyl)coumarin,[35] were prepared as referenced.

Analytical data of final compounds **2-40**, **42**, **43**, **45** are reported in Table 6. Analytical details and spectroscopic data of all the intermediates **1a-k** and final compounds are available as Supporting Information.

General procedure for the synthesis of 7-(ω-bromoalkyloxy)-3,4-dimethylcoumarins 1a-d, 7-(3-(bromomethyl)benzyloxy)coumarin 1e and 7-(4-(bromomethyl)benzyloxy)-3,4-substituted coumarins 1f-k.

A Pyrex vessel was charged with a magnetic stirring bar, and then the appropriate 7-hydroxycoumarin derivative (5.0 mmol) and potassium carbonate (0.70 g, 5.0 mmol) were

suspended in dry acetonitrile (20 mL). The suitable commercially available dibromo-derivative (1,ω-dibromoalkane or α,α'-dibromo-*m*-xylene or α,α'-dibromo-*p*-xylene, 25 mmol) was added. The reactor was placed in a microwave apparatus and irradiated at 130 °C for 30 min. After cooling to room temperature, the solid residue was filtered and washed with dichloromethane. The solution was concentrated to dryness and the resulting crude was purified through flash chromatography (gradient eluent, different mixtures of ethyl acetate in *n*-hexane).

2-(4-(Bromomethyl)phenyl)ethanol (41a). (4-Bromomethyl)phenylacetic acid (0.60 g, 2.6 mmol) was dissolved under magnetic stirring with 8 mL of anhydrous THF in a flame-dried round-bottomed flask kept to 0 °C. Borane·dimethyl sulfide (0.40 mL, 3.9 mmol) was then added dropwise and the mixture carefully cooled to room temperature and then left for additional 2 h. Water was cautiously added and the organic solvent was evaporated. Aqueous layer was extracted with ethyl acetate; the organic layers were collected, dried over sodium sulfate and evaporated to dryness to give the title product. Yield: 87%. ^{1}H NMR (DMSO-d_6) δ: 2.69 (t, J = 7.1 Hz, 2H), 3.57 (t, J = 7.1 Hz, 1H, exch. D_2O), 3.79-3.87 (m, 2H), 4.66 (s, 2H), 7.18 (d, J = 7.7 Hz, 2H), 7.33 (d, J = 7.7 Hz, 2H).

7-{[4-(2-Hydroxyethyl)benzyl]oxy}-2*H*-chromen-2-one (41b). A Pyrex vessel was charged with a magnetic stirring bar, and then 7-hydroxycoumarin (0.32 g, 2.0 mmol) and potassium carbonate (0.28 g, 2.0 mmol) were suspended in dry acetone (12 mL). Bromide **41a** (0.43 g, 2.0 mmol) was added and the reactor was placed in a microwave apparatus and irradiated at 130 °C for 30 min. After cooling to room temperature, the solid residue was filtered and washed with dichloromethane. The solution was concentrated to dryness and the resulting oil was purified through flash chromatography (gradient eluent, methanol in dichloromethane 0%→10%). Yield: 77%. ^{1}H NMR (DMSO-d_6) δ: 2.70 (t, J = 7.1 Hz, 2H), 3.56-3.61 (m, 2H), 4.59-4.63 (m, 1H,

exch. D_2O), 5.15 (s, 2H), 6.27 (d, J = 9.6 Hz, 1H), 6.98-7.06 (m, 2H), 7.35 (d, J = 8.0 Hz, 2H), 7.22 (d, J = 8.0 Hz, 2H), 7.62 (d, J = 8.5 Hz, 1H), 7.97 (d, J = 9.6 Hz, 1H).

7-(4-(2-Bromoethyl)benzyloxy)-2*H*-chromen-2-one (41c). Intermediate **41b** (0.40 g, 1.4 mmol) was dissolved in 5.0 mL of anhydrous dichloromethane under stirring with carbon tetrabromide (0.49 g, 1.5 mmol). To this mixture, a solution of triphenylphosphine (0.43 g, 1.6 mmol) in 5.0 mL of anhydrous dichloromethane was dropped at 0 °C and the resulting solution was kept at room temperature for 4 h. Evaporation of the solvent and purification by flash chromatography (gradient eluent, ethyl acetate in *n*-hexane 0%→60%) afforded bromide **41c**. Yield: 77% yield. ^{1}H NMR (DMSO-d_6) δ: 3.12 (t, J = 7.1 Hz, 2H), 3.72 (t, J = 7.1 Hz, 2H), 5.17 (s, 2H), 6.28 (d, J = 9.6 Hz, 1H), 7.00 (dd, J_1 = 8.5 Hz, J_2 = 2.5 Hz, 1H), 7.06 (d, J = 2.5 Hz, 1H), 7.29 (d, J = 8.0 Hz, 2H), 7.40 (d, J = 8.0 Hz, 2H), 7.62 (d, J = 8.5 Hz, 1H), 7.97 (d, J = 9.6 Hz, 1H).

(2*E*)-*N*-(3-Methoxyphenyl)-3-phenylacrylamide (44a). To a suspension of *trans*-cinnamic acid (0.89 g, 6.0 mmol) in dry dichloromethane (5.0 mL), thionyl chloride (5.0 mL) was added. The resulting reaction mixture was refluxed for 6 h and then concentrated to dryness. The oily residue was dissolved in dry dichloromethane (20 mL) and *m*-anisidine (0.67 mL, 6.0 mmol) was slowly added. After refluxing for 4 h, the solvent was evaporated under vacuum and the resulting crude was crystallized from hot ethanol. Yield: 70%. ^{1}H NMR (DMSO-d_6) δ: 3.73 (s, 3H), 6.61-6.66 (m, 1H), 6.81 (d, J = 15.7 Hz, 1H), 7.18-7.25 (m, 2H), 7.36-7.46 (m, 4H), 7.53-7.62 (m, 3H), 10.17 (s, 1H, exch, D_2O).

7-Hydroxy-2-quinolinone (44b).[70] Phenylacrylamide **44a** (0.63 g, 2.5 mmol) was dissolved in chlorobenzene (12 mL) in a flame-dried round-bottomed flask. $AlCl_3$ (1.3 g, 10 mmol) was added portionwise while cooling to 0 °C. The reaction mixture was refluxed for 8 h, then cooled

and poured into crushed ice. The resulting precipitate was washed with chloroform followed by diethyl ether, thus yielding the desired intermediate. Yield: 67%. ^{1}H NMR (DMSO-d_6) δ: 6.19 (d, J = 9.3 Hz, 1H), 6.59-6.71 (m, 2H), 7.42 (d, J = 8.3 Hz, 1H), 7.72 (d, J = 9.3 Hz, 1H), 10.08 (s, 1H, exch. D_2O), 11.48 (s, 1H, exch. D_2O).

7-(4-(Bromomethyl)benzyloxy)-2*H*-quinolin-2-one (44c). In a Pyrex vessel charged with a magnetic and a Weflon stirring bar, phenol **44b** (0.24 g, 1.5 mmol) and potassium carbonate (0.21 g, 1.5 mmol) were suspended in dry acetone (10 mL). α,α'-Dibromo-*p*-xylene (1.2 g, 4.5 mmol) was added and the reactor was placed in a microwave apparatus and irradiated at 130 °C for 30 min. After cooling to room temperature, the solid residue was filtered-off and washed with dichloromethane. The solution was concentrated to dryness and the resulting crude solid was purified through flash chromatography (gradient eluent, methanol in dichloromethane 0%→10%). Yield: 49%.^{1}H NMR (DMSO-d_6) δ: 4.71 (s, 2H), 5.13 (s, 2H), 6.28 (d, J = 9.3 Hz, 1H), 6.84-6.85 (m, 2H), 7.40-7.57 (m, 5H), 7.78 (d, J = 9.3 Hz, 1H), 11.60 (brs, 1H, exch. D_2O).

General procedure for the synthesis of final compounds 2-40, **42**, **43**, **45**

Appropriate bromide **1a-k**, **41c** or **44c** (0.50 mmol) were suspended under magnetic stirring in 4.0 mL of anhydrous acetonitrile in a Pyrex microwave reactor in the presence of potassium carbonate (0.64 g, 0.50 mmol) and a catalytic amount of potassium iodide (for compounds **2-12** and **42-43**). Benzylamine (2.5 mmol), suitable substituted *N*-methylbenzylamine[81,82] (0.75 mmol) or *N*-ethylbenzylamine (0.75 mmol) was added. The vessel was placed in a microwave apparatus and heated at 130 °C for 30 min. After cooling to room temperature, the reaction mixture was poured into ice-cold water (50 g) and extracted with dichloromethane (3 x 20 mL). The organic fractions were collected, dried over anhydrous sodium sulfate and evaporated to dryness, to give a residue that was crystallized from an appropriate solvent (as indicated in the Supporting

Information) or purified by flash chromatography (gradient eluent: different mixtures of methanol in dichloromethane or ethyl acetate in *n*-hexane). Compounds **2**, **3**, **7**-**10** and **12** were crystallized as hydrochlorides by treatment with HCl 1.25 N in ethanol. Compounds **5**, **14**, **16**-**18**, **22**-**37**, **39**-**40**, **42**, **43** and **45** were transformed into the corresponding hydrochloride salts by treating the crude oil with HCl 4.0 N in 1,4-dioxane (commercially available) or by dissolving the solid crude in the minimum volume of 1,4-dioxane before adding HCl 4.0 N in 1,4-dioxane.

Rat and Human Monoamine Oxidases Inhibition Assays.

rMAO inhibitory activity of compounds in Tables 1-3 was assessed using a continuous spectrophotometric assay,[83] monitoring the rate of oxidation of the nonselective nonfluorescent MAO substrate kynuramine to 4-hydroxyquinoline. MAO-A and MAO-B activities in rat mitochondrial preparations were assayed using as the controls the selective and irreversible inhibitors clorgyline (250 nM) and (−)-L-deprenyl (250 nM), respectively. IC_{50} values were determined by nonlinear regression of MAO inhibition vs. −log of the concentration plots, using the program Origin, version 6.0 (Microcal Software Inc., Northampton, MA).

Human monoamine oxidase inhibition assays were carried out with a fluorescence based method,[72] also using kynuramine as non-selective substrate of MAO-A and MAO-B. Briefly, reactions were performed in triplicate in black, flat-bottomed polystyrene 96-well microtiter plates (FluoroNunc/LumiNund, MaxiSorpTM surface, NUNC, Roskild, Denmark) containing potassium phosphate buffer (158 μL), an aqueous stock solution of kynuramine 0.5 mM (final kynuramine concentration corresponding to 50 μM), and DMSO solution of inhibitor in final concentrations ranging from 10^{-4} to 10^{-11} M. Samples were incubated at 37 °C, and then diluted human recombinant MAO-A and MAO-B (Supersomes; BD Gentest, Woburn, MA) were delivered to obtain final protein concentrations of 0.009 mg/mL and 0.015 mg/mL, respectively.

Incubation was carried out at 37 °C for 30 min, and then the reactions were stopped by addition of 75 μL of 2N NaOH.

Formation of 4-hydroxyquinoline was quantified with a 96-well microplate fluorescence reader (FLx 800, BioTek Instruments, Inc. Winoosli, USA) at excitation/emission wavelengths of 310/400 nm (20 nm slit width for excitation, 30 nm slit width for emission). Inhibitory activities (IC_{50}s) were determined by means of non-linear regressions performed with GraphPad Prism 5.0 software. Results are the mean of at least two independent experiments.

Electric Eel, Equine Serum and Human Cholinesterases Inhibition Assays

The spectrophotometric Ellman's test[71] for in vitro inhibition assay of AChE from electric eel (463 U/mg; Sigma) and BChE from equine serum (13 U/mg; Sigma) was followed as previously described.[24] The concentration of compound which determined 50% inhibition of the cholinesterase activity (IC_{50}) was calculated by nonlinear regression of the response/log(concentration) curve, using GraphPad Prism version 5. Kinetic studies were performed with the same test conditions, using six concentrations of substrate (from 0.033 to 0.2 mM) and four concentrations of inhibitor (0 to 0.25 μM). Apparent inhibition constants and kinetic parameters were calculated within the 'Enzyme kinetics' module of Prism. Inhibition tests on human recombinant AChE (2770 U/mg; Sigma) and BChE from human serum (50 U/mg; Sigma) were run under the same experimental conditions used for eeAChE.

Bi-directional Transport Studies on MDCKII-MDR1 Monolayers

MDCKII-MDR1 cells were cultured in DMEM medium and seeded at a density of 100000 cell/cm^2 onto polyester 12 well Transwell inserts (pore size 0.4 μm, 12 mm diameter, apical volume 0.5 mL, basolateral volume 1.5 mL). MDCKII-MDR1 cell barrier function was verified prior to the described transport experiments by means of trans-epithelial electrical resistance

(TEER) using an EVOM apparatus, and the measurement of the flux of fluorescein isothiocyanate-dextran (FD4, Sigma Aldrich, Italy) (200 μg/mL) and diazepam (75 μM). The TEER was measured in growth media (DMEM) at room temperature and calculated as the measured resistance minus the resistance of an empty Transwell (blank without cells). Cell monolayers with TEER values 800 Ohm/cm^2 were used. Following the TEER measurements, the cells were equilibrated in transport medium in both the apical and basolateral chambers for 30 minutes at 37 °C. The composition of transport medium was as follows: 0.4 mM K_2HPO_4, 25 mM $NaHCO_3$, 3 mM KCl, 122 mM NaCl, 10 mM glucose, pH = 7.4, and osmolarity 300 mOsm as determined by a freeze point based osmometer. At time 0, culture medium was aspirated from both the AP and BL chambers of each insert, and cell monolayers were washed three times (10 min per wash) with Dulbecco's Phosphate Buffered Saline (DPBS) pH = 7.4. Finally, a solution of compound diluted in transport medium was added to the apical or basolateral chamber. For AP-to-BL or BL-to-AP flux studies, the drug solution was added in the AP chamber or in the BL chamber, respectively. Except for FD4, which was solubilized directly in the assay medium at a concentration of 200 μg/mL, the other compounds were first dissolved in DMSO and then diluted with the assay medium to a final concentration of 75 μM. Next, the tested solutions were added to the donor side (0.5 mL for the AP chamber and 1.5 mL for the BL chamber) and fresh assay medium was placed in the receiver compartment. The percentage of DMSO never exceeded 1% (v/v) in the samples. The transport experiments were carried out under cell culture conditions (37 °C, 5% CO_2, 95% humidity). After incubation time of 120 min, samples were removed from the apical and basolateral side of the monolayer and then stored until further analysis.

Quantitative analysis of compounds **37** and diazepam were performed through UV–visible (Vis) spectroscopy using a PerkinElmer double-beam UV–visible spectrophotometer Lambda Bio 20 (Milan, Italy), equipped with 10 mm path-length-matched quartz cells. Standard calibration curves were prepared at maximum absorption wavelength of each compound using PBS as solvent and were linear ($r^2 = 0.999$) over the range of tested concentration (from 5 to 100 μM). The FD4 samples were analyzed with a Victor3 fluorimeter (Wallac Victor3, 1420 Multilabel Counter, Perkin-Elmer) at excitation and emission wavelengths of 485 and 535 nm, respectively. Each compound was tested in triplicate, and the experiments were repeated three times.

The apparent permeability, in units of cm/sec, was calculated using the following equation:

$$P_{app} = \left(\frac{V_A}{area \times time}\right) \times \left(\frac{[drug]_{acceptor}}{[drug]_{initial}}\right)$$

where "VA" is the volume in the acceptor well, "area" is the surface area of the membrane, "time" is the total transport time, "$[drug]_{acceptor}$" is the concentration of the drug measured by UV-spectroscopy and "$[drug]_{initial}$" is the initial drug concentration in the AP or BL chamber. Efflux ratio (ER) was calculated using the following equation: ER = P_{app}, BL-AP / P_{app}, AP-BL, where P_{app}, BL-AP is the apparent permeability of basal-to-apical transport, and P_{app}, AP-BL is the apparent permeability of apical-to-basal transport. An efflux ratio greater than 2 indicates that a test compound is likely to be a substrate for P-gp transport.

Cytotoxicity Assays

Human neuroblastoma cells SH-SY5Y were maintained at 37 °C in a humidified incubator containing 5% CO_2 in DMEM nutrient (Lonza) supplemented with 10% heat inactivated FBS, 2

mM L-glutamine, 100 U/mL penicillin and 100 μg/mL streptomycin. Cells were dispensed into 96-well microtiter plates at a density of 10000 cells/well. Following overnight incubation, cells were treated with a range of compound concentrations (0.1-50 μM). Then the plates were incubated at 37 °C for 24, 48 and 72 h. An amount of 10 μL of 0.5% w/v MTT was further added to each well and the plates were incubated for an additional 3 h at 37 °C. Finally the cells were lysed by addition of 100 μL of DMSO/EtOH 1:1 (v/v) solution. The absorbance at 570 nm was determined using a Perkin Elmer 2030 multilabel reader Victor TM X3.

Neuroprotection against oxidative stress

Human neuroblastoma SH-SY5Y cells were dispensed into 96-well microtiter plates at a density of 10000 cells/well. Following overnight incubation, cells were treated with a range of compound concentrations (1 and 10 μM at time zero and maintained for 24 h. Then, the media were replaced by fresh media still containing the drug plus the cytotoxic stimulus represented by 60 μM H_2O_2 that was left for an additional 24 h period. Thereafter, cell survival was determined using the 3-(4,5-dimethylthiazol-2-yl)-2,5-diphenyl-tetrazolium bromide (MTT) assay. The putative cytotoxic effects of **37** and of H_2O_2 were studied by exposing the cells to the compound at the highest concentration used in the neuroprotection studies for 24 h. Each compound was tested in triplicate, and the experiments were repeated three times. Statistical significance was assigned to $p < 0.01$ and calculated using a one-way analysis of variance (ANOVA) followed by the Bonferroni post hoc tests (GraphPad Prism vers. 5). Where indicated, standard error of the mean (SD) for data points has been calculated and the number of experiments is given (n).

Molecular docking

GOLD (vers. 5.2), a genetic algorithm-based software was used for the docking study. ChemPLP was selected as a fitness function. Automatic genetic algorithm parameter settings were used. All the crystal structures used in docking simulations were retrieved from the Protein Data Bank. In particular, the entry codes 1EVE and 4EY7 were downloaded for modeling hAChE and TcAChE, respectively; the entry codes 2V60 was downloaded for hMAO-B whereas a previously built homology modeling was used for rMAO-B.[47] The Protein Preparation Wizard available from Schroedinger[84] was used for the protein pretreatment in order to add missing hydrogen atoms, define the protonation states at pH equal to 7.4 and tautomers for histidine residues and to soft-minimize the whole structure. For each simulation, 10 conformations were generated for each inhibitor in a sphere of a 17 Å, using as references the centroids of ligand co-crystallized in 1EVE and 2V60. In MAO docking runs, the X-ray coordinates of 7-(3-chlorobenzyloxy)-4-carboxaldehyde-coumarin taken from 2V60 were used as scaffold constrain to bias binding mode towards MAO-B. In addition, the side chains of Glu206, Tyr112, Asn116 and His115 (mutated to Tyr115 in the case of rMAO-B) were set be flexible. Finally, eight ordered water molecules were explicitly taken into account in docking runs, as elsewhere reported.[68]

ASSOCIATED CONTENT

Supporting Information. Analytical and spectroscopic (^{1}H NMR) data for intermediates **1a-k** and final compounds **2**-**40**, **42**, **43** and **45** are reported separately as Supporting Information. This material is available free of charge via the Internet at http://pubs.acs.org.

AUTHOR INFORMATION

Corresponding Authors

*To whom correspondence should be addressed:

Angelo Carotti: phone +39 080 5442782; fax +39 080 5442230; email angelo.carotti@uniba.it

Marco Catto: phone +39 080 5442803; fax +39 080 5442230; email marco.catto@uniba.it

Present Addresses

† Ensemble Therapeutics, 99 Erie St, Cambridge MA 02139, USA.

Author Contributions

All authors contributed to the writing of the manuscript, gave approval to the final version of the manuscript and declared no conflict of interest.

ACKNOWLEDGMENTS

The authors thank MIUR (Rome, Italy) for partial financial support.

ABBREVIATIONS

3D-QSAR, three-dimensional quantitative structure-activity relationships; Aβ, beta amyloid protein; ACh, acetylcholine; AChE, acetylcholinesterase; AChEI, AChE inhibitors; AD,

Alzheimer's disease; BBB, blood brain barrier; BChE, butyrylcholinesterase; CAS, catalytic anionic binding site; DBS, dual binding site; DMEM, Dulbecco's modified eagle medium; ER, efflux ratio; ESI-MS, electrospray ionization mass spectrometry; FAD, flavin adenine dinucleotide; FD4, fluorescein isothiocyanate-dextran; MAO-A, monoamine oxidase A; MAO-B, monoamine oxidase B; MTT, 3-(4,5-dimethylthiazol-2-yl)-2,5-diphenyltetrazolium bromide; ND, neurodegenerative disease; NMDA, N-methyl-D-aspartate; P_{app}, apparent permeability; P_{app} AP-BL, apparent permeability apical-to-basal; P_{app} BL-AP, apparent permeability basal-to-apical; PAS, peripheral anionic binding site; PD, Parkinson's disease; P-gp, P-glycoprotein; ROS, reactive oxygen species; SAR, structure-activity relationships; SSR, structure-selectivity relationships; TEER, trans-epithelial electrical resistance.

REFERENCES

(1) a) Banerjee, S. The Macroeconomics of Dementia-Will the World Economy get Alzheimer's Disease? *Arch. Med. Res.* **2012**, *43*, 705-709. b) Narayan, P.; Ehsani, S.; Lindquist, S. Combating Neurodegenerative Disease with Chemical Probes and Model Systems. *Nat. Chem. Biol.* **2014**, *10*, 911-920.

(2) Trippier, P. C.; Labby, K. J.; Hawker, D. D.; Mataka, J. J.; Silverman, R. B. Target- and Mechanism-Based Therapeutics for Neurodegenerative Diseases: Strength in Numbers. *J. Med. Chem.* **2013**, *56*, 3121−3147.

(3) Alzheimer's Association, 2015 Alzheimer's disease facts and figures. *Alzheimer's Dement.* **2015**, *11*, 332-384.

(4) Misra, S.; Medhi, B. Drug Development Status for Alzheimer's Disease: Present Scenario. *Neurol. Sci.* **2013**, *34*, 831-839.

(5) Berk, C.; Sabbagh, M. N. Successes and Failures for Drugs in Late-stage Development for Alzheimer's Disease. *Drugs Aging* **2013**, *10*, 783-792.

(6) Querfurth, H. W.; LaFerla, F. M. Alzheimer's Disease. *N. Engl. J. Med.* **2010**, *362*, 329-344.

(7) Chakrabarti, S.; Sinha, M.; Thakurta, I. G.; Banerjee, P.; Chattopadhyay, M. Oxidative Stress and Amyloid Beta Toxicity in Alzheimer's Disease: Intervention in a Complex Relationship by Antioxidants. *Curr. Med. Chem.* **2013**, *20*, 4648-4664.

(8) Terry, A. V.; Buccafusco, J. J. The Cholinergic Hypothesis of Age and Alzheimer's Disease-related Cognitive Deficits: Recent Challenges and Their Implications for Novel Drug Development. *J. Pharmacol. Exp. Ther.* **2003**, *306*, 821–827.

(9) Anand, P.; Singh, B. A Review on Cholinesterase Inhibitors for Alzheimer's Disease. *Arch. Pharm. Res.* **2013**, *36*, 375-399.

(10) Cheewakriengkrai, L.; Gauthier, S. A 10-Year Perspective on Donepezil. *Expert Opin. Pharmacother.* **2013**, *14*, 331-338.

(11) Lo, D.; Grossberg, G. T. Use of Memantine for the Treatment of Dementia. *Expert Rev. Neurother.* **2011**, *11*, 1359-1370.

(12) Darvesh, S.; Hopkins, D. A.; Geula, C. Neurobiology of Butyrylcholinesterase. *Nat. Rev. Neurosci.* **2003**, *2*, 131–138.

(13) Harel, M.; Schalk, I.; Ehret-Sabatier, L.; Bouet, F.; Goeldner, M.; Hirth, C.; Axelsen, P. H.; Silman, I.; Sussman, J. L. Quaternary Ligand Binding to Aromatic Residues in the Active-site Gorge of Acetylcholinesterase. *Proc. Nat. Acad. Sci. U.S.A.* **1993**, *90*, 9031–9035.

(14) Kryger, G.; Silman, I.; Sussman, J. L. Structure of Acetylcholinesterase Complexed with E2020 (Aricept): Implications for the Design of New Anti-Alzheimer Drugs. *Structure* **1999**, *7*, 297–307.

(15) Tarozzi, A.; Bartolini, M.; Piazzi, L.; Valgimigli, L.; Amorati, R.; Bolondi, C.; Djemil, A.; Mancini, F.; Andrisano, V.; Rampa, A. From the Dual Function Lead AP2238 to AP2469, a Multi-target-directed Ligand for the Treatment of Alzheimer's Disease. *Pharmacol. Res. Perspect.* **2014**, *2*, e00023.

(16) Dvira, H.; Silman, I.; Harel, M.; Rosenberry, T. L.; Sussman, J. L. Acetylcholinesterase: From 3D Structure to Function. *Chem. Biol. Interact.* **2010**, *187*, 10–22.

(17) Pisani, L.; Catto, M.; Giangreco, I.; Leonetti, F.; Nicolotti, O.; Stefanachi, A.; Cellamare, S.; Carotti, A. Design, Synthesis and Biological Evaluation of Coumarin Derivatives Tethered to an Edrophonium-like Fragment as Highly Potent and Selective Dual Binding Site Acetylcholinesterase Inhibitors. *ChemMedChem* **2010**, *5*, 1616–1630.

(18) Catto, M.; Pisani, L.; Leonetti, F.; Nicolotti, O.; Pesce, P.; Stefanachi, A.; Cellamare, S.; Carotti, A. Design, Synthesis and Biological Evaluation of Coumarin Alkylamines as Potent and Selective Dual Binding Site Inhibitors of Acetylcholinesterase. *Bioorg. Med. Chem.* **2013**, *21*, 146-152.

(19) Leonetti, F.; Catto, M.; Nicolotti, O.; Pisani, L.; Cappa, A.; Stefanachi, A.; Carotti, A. Homo- and Hetero-Bivalent Edrophonium-like Ammonium Salts as Highly Potent, Dual Binding Site AChE Inhibitors. *Bioorg. Med. Chem.* **2008**, *16*, 7450–7456.

(20) Conejo-Garcia, A.; Pisani, L.; del Carmen Nunez, M.; Catto, M.; Nicolotti, O.; Leonetti, F.; Campos, J. M.; Gallo, M. A.; Espinosa, A.; Carotti, A. Homodimeric Bis-Quaternary Heterocyclic Ammonium Salts as Potent Acetyl- and Butyrylcholinesterase Inhibitors: A Systematic Investigation of the Influence of Linker and Cationic Heads over Affinity and Selectivity. *J. Med. Chem.* **2011**, *54*, 2627–2645.

(21) Nicolotti, O.; Pisani, L.; Catto, M.; Leonetti, F.; Giangreco, I.; Stefanachi, A.; Carotti, A. Discovery of a Potent and Selective Hetero-bivalent AChE Inhibitor via Bioisosteric Replacement. *Mol. Inform*. **2011**, *30*, 133-136.

(22) Carotti, A.; De Candia, M.; Catto, M.; Borisova, T. N.; Varlamov, A. V.; Mendez-Alvarez, E.; Soto-Otero, R.; Voskressensky, L. G.; Altomare, C. Ester Derivatives of Annulated Tetrahydroazocines: a New Class of Selective Acetylcholinesterase Inhibitors. *Bioorg. Med. Chem*. **2006**, *14*, 7205-7212.

(23) Tasso, B.; Catto, M.; Nicolotti, O.; Novelli, F.; Tonelli, M.; Giangreco, I.; Pisani, L.; Sparatore, A.; Boido, V.; Carotti, A.; Sparatore, F. Quinolizidinyl Derivatives of Bi- and Tricyclic Systems as Potent Inhibitors of Acetyl- and Butyrylcholinesterase with Potential in Alzheimer's Disease. *Eur. J. Med. Chem.* **2011**, *46*, 2170-2184.

(24) Catto, M.; Berezin, A. A.; Lo Re, D.; Loizou, G.; Demetriades, M.; De Stradis, A.; Campagna, F.; Koutentis, P. A.; Carotti, A. Design, Synthesis and Biological Evaluation of Benzo[e][1,2,4]triazin-7(1H)-one and [1,2,4]-Triazino[5,6,1-jk]carbazol-6-one Derivatives as Dual Inhibitors of Beta-amyloid Aggregation and Acetyl/butyryl Cholinesterase. *Eur. J. Med. Chem.* **2012**, *58*, 84-97.

(25) Youdim, M. B.; Edmondson, D.; Tipton, K. F. The Therapeutic Potential of Monoamine Oxidase Inhibitors. *Nat. Rev. Neurosci.* **2006**, *7*, 295−309.

(26) Edmondson, D.E.; Mattevi, A.; Binda, C.; Li, M.; Hubalek, F. Structure and Mechanism of Monoamine Oxidases. *Curr. Med. Chem.* **2004**, *11*, 1983-1993.

(27) Grimsby, J.; Lan, N. C.; Neve, R.; Chen, K.; Shih, J. C. Tissue Distribution of Human Monoamine Oxidase-A and Oxidase-B Messenger-RNA. *J. Neurochem.* **1990**, *55*, 1166−1169.

(28) Fowler, C.J.; Ross, S.B. Selective Inhibitors of Monoamine Oxidase A and B: Biochemical, Pharmacological, and Clinical Properties. *Med. Res. Rev.* **1984**, *4*, 323-358.

(29) Pisani, L.; Catto, M.; Leonetti, F.; Nicolotti, O.; Stefanachi, A.; Campagna, F.; Carotti, A. Targeting Monoamine Oxidases with Multipotent Ligands: An Emerging Strategy in the Search of New Drugs Against Neurodegenerative Diseases. *Curr. Med. Chem.* **2011**, *18*, 4568-4587.

(30) Salat, D.; Tolosa, E. Levodopa in the Treatment of Parkinson's Disease: Current Status and New Developments. *J. Parkinson's Dis.* **2013**, *3*, 255-269.

(31) De Colibus, L.; Li, M.; Binda, C.; Lustig, A.; Edmondson, D. E.; Mattevi, A. Three-Dimensional Structure of Human Monoamine Oxidase A (MAO-A): Relation to the Structures of Rat MAO-A and Human MAO-B. *Proc. Natl. Acad. Sci. U.S.A.* **2005**, *102*, 12684−12689.

(32) Son, S.-Y.; Jichun, Ma, J.; Kondou, Y.; Yoshimura, M.; Yamashita, E.; Tsukihara, T. Structure of Human Monoamine Oxidase A at 2.2-Å Resolution: The Control of Opening the Entry for Substrates/inhibitors. *Proc. Natl. Acad. Sci. U.S.A.* **2008**, *105*, 5739−5744.

(33) Binda, C.; Newton-Vinson, P.; Hubalek, F.; Edmondson, D. E.; Mattevi, A. Structure of Human Monoamine Oxidase B, a Drug Target for the Treatment of Neurological Disorders. *Nat. Struct. Mol. Biol.* **2002**, *9*, 22−26.

(34) Binda, C.; Hubalek, F.; Li, M.; Herzig, Y.; Sterling, J.; Edmondson, D. E.; Mattevi, A. Crystal Structures of Monoamine Oxidase B in Complex with Four Inhibitors of the N-Propargylaminoindan Class. *J. Med. Chem.* **2004**, *47*, 1767-1774.

(35) Binda, C.; Wang, J.; Pisani, L.; Caccia, C.; Carotti, A.; Salvati, P.; Edmondson, D. E.; Mattevi, A. Structures of Human Monoamine Oxidase B Complexes with Selective Noncovalent Inhibitors: Safinamide and Coumarin Analogs. *J. Med. Chem.* **2007**, *50*, 5848-5852.

(36) Riederer, P.; Danielczyk, W.; Gruenblatt, E. Monoamine Oxidase-B Inhibition in Alzheimer's Disease. *Neurotoxicology* **2004**, *1-2*, 271-277.

(37) Qureshi, I. A.; Mehler, M. F. Advances in Epigenetics and Epigenomics for Neurodegenerative Diseases. *Curr. Neurol. Neurosci. Rep.* **2011**, *11*, 464-473.

(38) Leon, R.; Garcia, A. G.; Marco-Contelles, J. Recent Advances in the Multitarget-Directed Ligands Approach for the Treatment of Alzheimer's Disease. *Med. Res. Rev.* **2013**, *33*, 139-189.

(39) Morphy, J. R.; Harris, C. J. *Designing Multi-Target Drugs*. RSC Publishing: London 2012.

(40) Youdim, M. B.; Buccafusco, J. J. CNS Targets for Multi-functional Drugs in the Treatment of Alzheimer's and Parkinson's Diseases. *J. Neural Transm.* **2005**, *112*, 519-537.

(41) Buccafusco, J. J.; Terry, A. V. Jr. Multiple Central Nervous System Targets for Eliciting Beneficial Effects on Memory and Cognition. *J. Pharmacol. Exp. Ther.* **2000**, *295*, 438-446.

(42) Nicolotti, O.; Giangreco, I.; Introcaso, A.; Leonetti, F.; Stefanachi, A., Carotti, A. Strategies of Multi-Objective Optimization in Drug Discovery and Development. *Expert Opin. Drug Discovery* **2011**, *6*, 871-884.

(43) Kneubuehler, S.; Thull, U.; Altomare, C.; Carta, V.; Gaillard, P.; Carrupt, P. A.; Carotti, A.; Testa, B. Inhibition of Monoamine Oxidase-B by 5H-Indeno[1,2-c]pyridazines: Biological Activities, Quantitative Structure−Activity Relationships (QSARs) and 3DQSARs. *J. Med. Chem.* **1995**, *38*, 3874−3883.

(44) Gnerre, C.; Catto, M.; Leonetti, F.; Weber, P.; Carrupt, P.-A.; Altomare, C.; Carotti, A.; Testa, B. Inhibition of Monoamine Oxidases by Functionalized Coumarin Derivatives: Biological Activities, QSARs, and 3D-QSARs. *J. Med. Chem.* **2000**, *43*, 4747−4758.

(45) Catto, M.; Nicolotti, O.; Leonetti, F.; Carotti, A.; Favia, A. D.; Soto-Otero, R.; Mendez-Alvarez, E.; Carotti, A. Structural Insights into Monoamine Oxidase Inhibitory Potency and Selectivity of 7-Substituted Coumarins from Ligand- and Target-Based Approaches. *J. Med. Chem.* **2006**, *49*, 4912−4925.

(46) Carotti, A.; Melloni, P.; Thaler, F.; Caccia, C.; Maestroni, S.; Salvati, P. Substituted Aminoalkyl and Amidoalkyl Benzopyran Derivatives. WO 2006/102958 A1, 2006.

(47) Carotti, A.; Catto, M.; Leonetti, F.; Campagna, F.; Soto-Otero, R.; Mendez-Alvarez, E.; Thull, U.; Testa, B.; Altomare, C. Synthesis and Monoamine Oxidase Inhibitory Activity of New Pyridazine-,Pyrimidine- and 1,2,4-Triazine-Containing Tricyclic Derivatives. *J. Med. Chem.* **2007**, *22*, 5364−5371.

(48) Leonetti, F.; Capaldi, C.; Pisani, L.; Nicolotti, O.; Muncipinto, G.; Stefanachi, A.; Cellamare, S.; Caccia, C.; Carotti, A. Solid-Phase Synthesis and Insights into Structure−Activity Relationships of Safinamide Analogues as Potent and Selective Inhibitors of Type B Monoamine Oxidase. *J. Med. Chem.* **2007**, *50*, 4909−4916.

(49) Pisani, L.; Muncipinto, G.; Miscioscia, T. F.; Nicolotti, O.; Leonetti, F.; Catto, M.; Caccia, C.; Salvati, P.; Soto-Otero, R.; Mendez-Alvarez, E.; Passeleu, C.; Carotti, A. Discovery of a Novel Class of Potent Coumarin Monoamine Oxidase B Inhibitors: Development and Biopharmacological Profiling of 7-[(3-Chlorobenzyl)oxy]-4-[(methylamino)methyl]-2*H*-

chromen-2-one Methanesulfonate (NW-1772) as a Highly Potent, Selective, Reversible, and Orally Active Monoamine Oxidase B Inhibitor. *J. Med. Chem.* **2009**, *52*, 6685−6706.

(50) Pisani, L.; Barletta, M.; Soto-Otero, R.; Nicolotti, O.; Mendez-Alvarez, E.; Catto, M.; Introcaso, A.; Stefanachi, A.; Cellamare, S.; Altomare, C.; Carotti, A. Discovery, Biological Evaluation, and Structure−Activity and −Selectivity Relationships of 6'-Substituted (E)‑2-(Benzofuran-3(2*H*)‑ylidene)‑*N*‑methylacetamides, a Novel Class of Potent and Selective Monoamine Oxidase Inhibitors. *J. Med. Chem.* **2013**, *56*, 2651–2664.

(51) Bruehlmann, C.; Ooms, F.; Carrupt, P. A.; Testa, B.; Catto, M.; Leonetti, F.; Altomare, C.; Carotti, A. Coumarin Derivatives as Dual Inhibitors of Acetylcholinesterase and Monoamine Oxidase. *J. Med. Chem.* **2001**, *44*, 3195-3198.

(52) Carotti, A. MAOs Long March: From Toxic First-Generation Drugs to Isoform-Selective, Reversible and Multi-Target Inhibitors. Frontiers in CNS and Oncology Medicinal Chemistry, ACS-EFMC, Siena, Italy, October 7−9 (2007), COMC-059. Publisher: American Chemical Society, Division of Medicinal Chemistry, Washington D. C. CODEN: 69KAR2.

(53) Sterling, J.; Herzig, Y.; Goren, T.; Finkelstein, N.; Lerner, D.; Goldenberg, W.; Miskolczi, I.; Molnar, S.; Rantal, F.; Tamas, T.; Toth, G.; Zagyva, A.; Zekany, A.; Lavian, G.; Gross, A.; Friedman, R.; Razin, M.; Huang, W.; Krais, B.; Chorev, M.; Youdim, M. B. H.; Weinstock, M. Novel Dual Inhibitors of AChE and MAO Derived from Hydroxy Aminoindan and Phenethylamine as Potential Treatment for Alzheimer's Disease. *J. Med. Chem.* **2002**, *45*, 5260−5279.

(54) Samadi, A.; de los Ríos, C.; Bolea, I.; Chioua, M.; Iriepa, I.; Moraleda, I.; Bartolini, M.; Andrisano, V.; Gálvez, E.; Valderas, C.; Unzeta, M.; Marco-Contelles, J. Multipotent MAO and Cholinesterase Inhibitors for the Treatment of Alzheimer's Disease: Synthesis, Pharmacological Analysis and Molecular Modeling of Heterocyclic Substituted Alkyl and Cycloalkyl Propargyl Amine. *Eur. J. Med. Chem.* **2012**, *52*, 251-262.

(55) Yanez, M.; Vina, D. Dual Inhibitors of Monoamine Oxidase and Cholinesterase for the Treatment of Alzheimer Disease. *Curr. Top. Med. Chem.* **2013**, *13*, 1692-1706.

(56) Passos, C. S.; Simões-Pires, C. A.; Nurisso, A.; Soldi, T. C.; Kato, L.; de Oliveira, C. M.; de Faria, E. O.; Marcourt, L.;Gottfried, C.; Carrupt, P.-A.; Henriques, A. T. Indole Alkaloids of Psychotria as Multifunctional Cholinesterases and Monoamine Oxidases Inhibitors. *Phytochemistry* **2013**, *86*, 8-20.

(57) Zheng, H.; Amit, T.; Bar-Am, O.; Fridkin, M.; Youdim, M. B. H.; Mandel, S. A. From Anti-Parkinson's Drug Rasagiline to Novel Multitarget Iron Chelators with Acetylcholinesterase and Monoamine Oxidase Inhibitory and Neuroprotective Properties for Alzheimer's Disease. *J. Alzheimer's Dis.* **2012**, *30*, 1-16.

(58) Bolea, I.; Gella, A.; Monjas, L.; Perez, C.; Rodriguez-Franco, M. I.; Marco-Contelles, J.; Samadi, A.; Unzeta, M. Multipotent, Permeable Drug ASS234 Inhibits Aβ Aggregation, Possesses Antioxidant Properties and Protects from Aβ-induced Apoptosis In Vitro. *Curr. Alzheimer Res.* **2013**, *10*, 797-808.

(59) Bautista-Aguilera, O. M.; Esteban, G.; Chioua, M.; Nikolic, K.; Agbaba, D.; Moraleda, I.; Iriepa, I.; Soriano, E.; Samadi, A.; Unzeta, M.; Marco-Contelles, J. Multipotent Cholinesterase/Monoamine Oxidase Inhibitors for the Treatment of Alzheimer's Disease:

Design, Synthesis, Biochemical Evaluation, ADMET, Molecular Modeling, and QSAR Analysis of Novel Donepezil-pyridyl Hybrids. *Drug Des. Devel. Ther.* **2014**, *8*, 1893–1910.

(60) Avramovich-Tirosh, Y.; Amit, T.; Bar-Am, O.; Zheng, H.; Fridkin, M.; Youdim, M.B.H. Therapeutic Targets and Potential of the Novel Brain Permeable Multifunctional Iron Chelator-Monoamine Oxidase Inhibitor Drug, M-30, for the Treatment of Alzheimer's Disease. *J. Neurochem.* **2007**, *100*, 490-502.

(61) Matos, M. J.; Pérez-Cruz, F.; Vazquez-Rodriguez, S.; Uriarte, E.; Santana, L.; Borges, F.; Olea-Azar, C. Remarkable Antioxidant Properties of a Series of Hydroxy-3-arylcoumarins. *Bioorg. Med. Chem.* **2013**, *21*, 3900-3906.

(62) Li, R. S.; Wang, X. B.; Hu, X. J.; Kong, L. Y. Design, Synthesis and Evaluation of Flavonoid Derivatives as Potential Multifunctional Acetylcholinesterase Inhibitors Against Alzheimer's disease. *Bioorg. Med. Chem. Lett*. **2013**, *23*, 2636–2641.

(63) Huang, L.; Lu, C.; Sun, Y.; Mao, F.; Luo, Z.; Su, T.; Jiang, H.; Shan, W.; Li, X. Multitarget-directed Benzylideneindanone Derivatives: Anti-β-Amyloid (Aβ) Aggregation, Antioxidant, Metal Chelation, and Monoamine Oxidase B (MAO-B) Inhibition Properties against Alzheimer's Disease. *J. Med. Chem.* **2012**, *55*, 8483-8492.

(64) Youdim, M.B.H.; Weinstock, M. Molecular Basis of Neuroprotective Activities of Rasagiline and the anti Alzheimer Drug, TV3326, [(N-Propargyl-(3R)-aminoindan-5-yl)-ethyl Methyl Carbamate]. *Cell. Mol. Neurobiol.* **2002**, *21*, 555-573.

(65) Anderson, M. C.; Hasan, F.; McCrodden, J. M.; Tipton, K. F. Monoamine Oxidase Inhibitors and the Cheese Effect. *Neurochem. Res.* **1993**, *18*, 1145−1149.

(66) Macdonald, I. R.; Rockwood, K.; Martin, E.; Darvesh, S. Cholinesterase Inhibition in Alzheimer's Disease: Is Specificity the Answer? *J. Alzheimer's Dis.* **2014**, *42*, 379-384

(67) Greig, N. H.; Utsuki, T.; Yu, Q.-S.; Zhu, X.; Holloway, H. W.; Perry, T. A.; Lee, B.; Ingram, D. H.; Lahiri, D. K. A New Therapeutic Target in AD Treatment: Attention to Butyrylcholinesterase. *Curr. Med. Res. Opin.* **2001**, *17*, 159-165.

(68) Pisani, L.; Catto, M.; Nicolotti, O., Grossi, G.; Di Braccio, M.; Soto-Otero, R.; Mendez-Alvarez, E.; Stefanachi, A.; Gadaleta, D.; Carotti, A. Fine Molecular Tuning at Position 4 of 2*H*-Chromen-2-one Derivatives in the Search of Potent and Selective Monoamine Oxidase B Inhibitors. *Eur. J. Med. Chem.* **2013**, *70*, 723-739.

(69) Pisani, L.; Farina, R.; Nicolotti, O.; Gadaleta, D.; Soto-Otero, R.; Catto, M.; Di Braccio, M.; Mendez-Alvarez, E.; Carotti A. In Silico Design of Novel 2*H*-Chromen-2-one Derivatives as Potent and Selective MAO-B Inhibitors. *Eur. J. Med. Chem.* **2015**, *89*, 98-105.

(70) Wang, T.-C.; Chen, Y.-L.; Lee, K.-H.; Tzeng, C.-C. Lewis Acid Catalyzed Reaction of Cinnamanilides: Competition of Intramolecular and Intermolecular Friedel-Crafts Reaction. *Synthesis* **1997**, *9*, 87-90.

(71) Ellman, G. L.; Courtney, K. D.; Andres, V., Jr.; Feartherstone, R. M. A New and Rapid Colorimetric Determination of Acetylcholinesterase Activity. *Biochem. Pharmacol.* **1961**, *7*, 88–95.

(72) Novaroli, L.; Daina, A.; Favre, E.; Bravo, J.; Carotti, A.; Leonetti, F.; Catto, M.; Carrupt, P.-A.; Reist, M. Impact of Species-dependent Differences on Screening, Design, and Development of MAO-B Inhibitors. *J. Med. Chem.* **2006**, *49*, 6264-6272.

(73) Denizot, F.; Lang, R. Rapid Colorimetric Assay for Cell Growth and Survival. Modifications to the Tetrazolium Dye Procedure Giving Improved Sensitivity and Reliability. *J. Immunol. Methods* **1986**, *89*, 271-277.

(74) Verdonk, M. L.; Cole, J. C.; Hartshorn, M. J.; Murray, C. W.; Taylor, R. D. Improved Protein-Ligand Docking Using GOLD. *Proteins* **2003**, *52*, 609-623.

(75) Liao, S.-M.; Du, Q.-S.; Meng, J.-Z.; Pang, Z.-W.; Huang, R.-B. The Multiple Roles of Histidine in Protein Interactions. *Chem. Cent. J.* **2013**, *7*, 44.

(76) Denora, N.; Laquintana, V.; Trapani, A.; Lopedota, A.; Latrofa, A.; Gallo, J. M.; Trapani, G. Translocator Protein (TSPO) Ligand-Ara-C (Cytarabine) Conjugates as a Strategy to Deliver Antineoplastic Drugs and to Enhance Drug Clinical Potential. *Mol. Pharm.* **2010**, *7*, 2255-2269.

(77) Inestrosa, N. C.; Alvarez, A.; Pérez, C. A.; Moreno, R. D.; Vicente, M.; Linker, C.; Casanueva, O. I.; Soto, C.; Garrido, J. Acetylcholinesterase Accelerates Assembly of Amyloid-Beta-Peptides into Alzheimer's Fibrils: Possible Role of the Peripheral Site of the Enzyme. *Neuron* **1996**, *16*, 881-891.

(78) Galdeano, C.; Viayna, E.; Arroyo, P.; Bidon-Chanal, A; Blas, J. R.; Muñoz-Torrero, D.; Luque, F. J. Structural Determinants of the Multifunctional Profile of Dual Binding Site Acetylcholinesterase Inhibitors as Anti-Alzheimer Agents. *Curr. Pharm. Des.* **2010**, *16*, 2818-2836.

(79) Denora, N.; Cassano, T.; Laquintana, V.; Lopalco, A.; Trapani, A.; Cimmino, C. S.; Laconca, L.; Giuffrida, A.; Trapani, G. Novel Codrugs with GABAergic Activity for Dopamine Delivery in the Brain. *Int. J. Pharm*. **2012**, *437*, 221-231.

(80) Fringuelli, F.; Piermatti, O.; Pizzo, F. One-pot Synthesis of 3-Carboxycoumarins via Consecutive Knoevenagel-Pinner Reactions in Water. *Synthesis* **2003**, *15*, 2331-2334.

(81) Piazzi, L.; Belluti, F.; Bisi, A.; Gobbi, S.; Rizzo, S.; Bartolini, M.; Andrisano, V.; Recanatini, M.; Rampa, A. Cholinesterase inhibitors: SAR and Enzyme Inhibitory Activity of 3-[ω-(Benzylmethylamino)alkoxy]xanthen-9-ones. *Bioorg. Med. Chem.* **2007**, *15*, 575-585.

(82) Kumpaty, H. J.; Williamson, J. S.; Bhattacharyya, S. Synthesis of *N*-Methyl Secondary Amines. *Synth. Commun.* **2003**, *33*, 1411-1416.

(83) Mendez-Alvarez, E.; Soto-Otero, R.; Sanchez-Sellero, I.; Lopez-Rivadulla, L. M.; Lamas, M. Inhibition of Brain Monoamine Oxidase by Adducts of 1,2,3,4-Tetrahydroisoquinoline with Components of Cigarette Smoke. *Life Sci.* **1997**, *60*, 1719−1727.

(84) Sastry, G. M.; Adzhigirey, M.; Day, T; Annabhimoju, R.; Sherman W. Protein and Ligand Preparation: Parameters, Protocols, and Influence on Virtual Screening Enrichments. *J. Comput.-Aided Mol. Des.* **2013**, *27*, 221-234.

Chart 1. Chemical structures of reference AChE and MAO inhibitors.

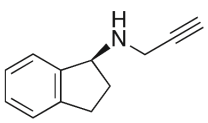

Rasagiline

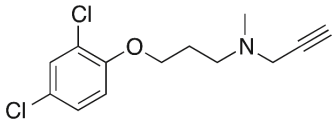

Clorgyline

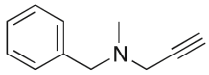

Pargyline

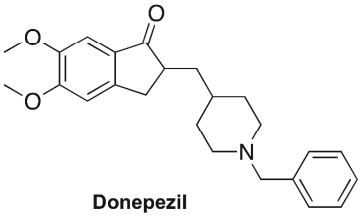

Donepezil

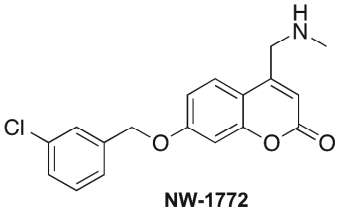

NW-1772

Scheme 1.[a] Synthesis of compounds **2-40**.

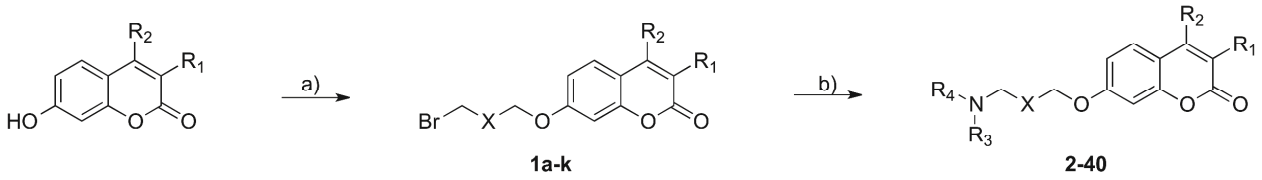

[a] Reagents and conditions: a) suitable dibromo-derivative (1,3-dibromopropane for **1a**, 1,4-dibromobutane for **1b**, 1,5-dibromopentane for **1c**, 1,6-dibromohexane for **1d**, α,α'-dibromo-*m*-xylene for **1e**, α,α'-dibromo-*p*-xylene for **1f-k**), K_2CO_3, dry acetonitrile, 30 min, 130 °C, MW; b) substituted benzylamine, K_2CO_3, KI (cat.) (for compounds **2-12**), dry acetonitrile, 30 min, 130 °C, MW.

Scheme 2.[a] Synthesis of compounds **42-43**.

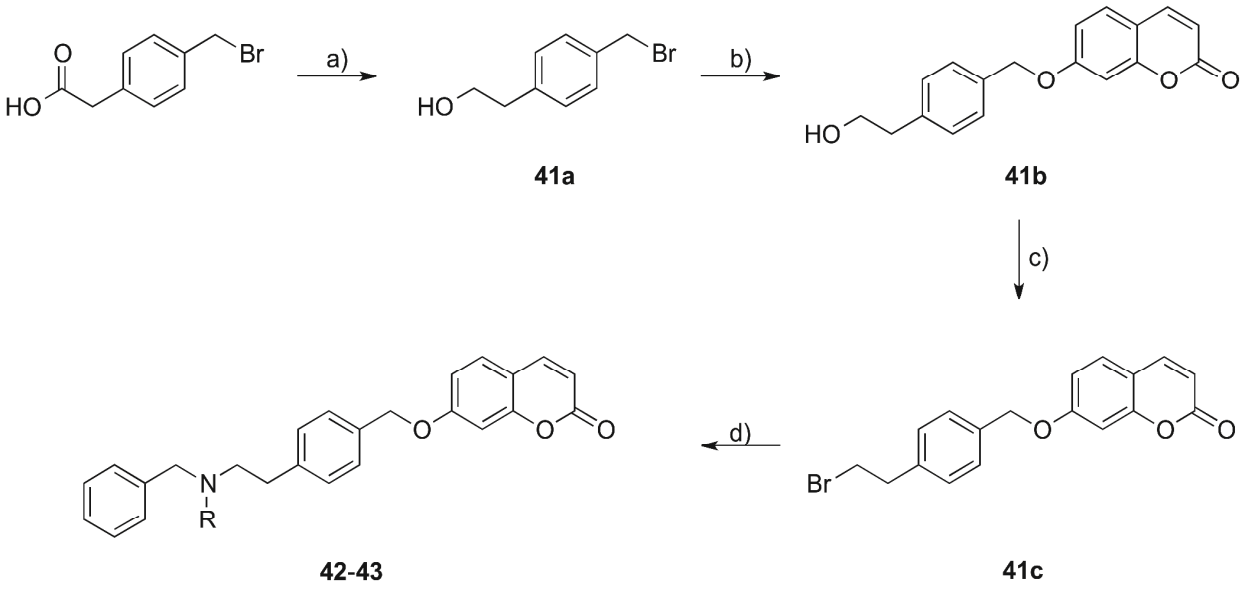

[a] Reagents and conditions: a) $BH_3 \cdot SMe_2$, THF, 0 °C to room temperature, 4 h; b) 7-hydroxycoumarin, K_2CO_3, dry acetonitrile, 130 °C, 30 min, MW; c) CBr_4, PPh_3, dry dichloromethane, 0 °C to room temperature, 4 h; d) benzylamine or *N*-benzylmethylamine, K_2CO_3, dry acetonitrile, KI (cat.), 130 °C, 30 min, MW.

Scheme 3.[a] Synthesis of compounds **45**

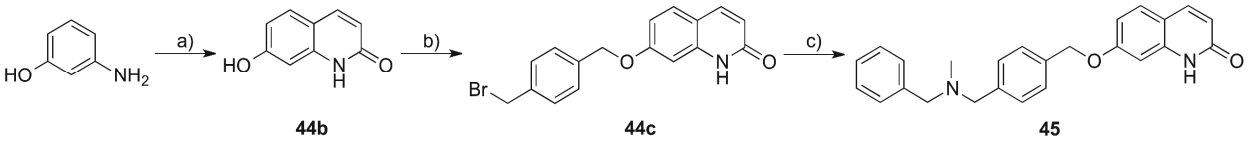

44b **44c** **45**

[a] Reagents and conditions: a) i: cinnamoyl chloride, dry dichloromethane, 4 h, reflux; ii: $AlCl_3$, chlorobenzene, 8 h, reflux; b) α,α'-dibromo-*p*-xylene, K_2CO_3, dry acetonitrile, 130 °C, 30 min, MW; c) *N*-methybenzylamine, K_2CO_3, dry acetonitrile, 130 °C, 30 min, MW.

Table 1. MAO and ChE inhibition data of coumarin derivatives **2-12**.

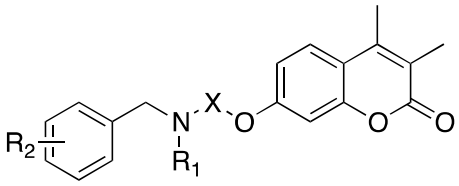

compd	X	R_1	R_2	IC_{50}, μM (or inhibition % at 10 μM)			
				MAO-A[a]	MAO-B[a]	AChE[b]	BChE[c]
2[d]	-$(CH_2)_3$-	Me	H	(35%)	0.33	1.3	7.8
3[d]		Et	H	7.4	0.98	0.36	4.0
4	-$(CH_2)_4$-	Me	H	6.6	1.1	0.49	3.7
5[d]	-$(CH_2)_5$-	H	H	2.2	0.50	0.94	1.8
6		Me	H	4.2	0.98	0.55	2.8
7[d]		Me	3-CN	5.3	2.5	2.3	4.1
8[d]		Me	3-Cl	(42%)	8.9	0.29	2.6
9[d]		Me	4-CN	(48%)	3.3	2.8	4.3
10[d]		Et	H	9.5	7.8	0.75	0.94
11	-$(CH_2)_6$-	Me	H	0.51	1.7	0.095	0.67
12[d]		Et	H	2.1	0.72	0.32	0.49

[a] From rat brain. [b] From electric eel. [c] from equine serum. Values are mean of two/three independent experiments; SEM < 10%. [d] Hydrochloride salt.

Table 2. MAO and ChE inhibition data of coumarin derivatives **13-40**.

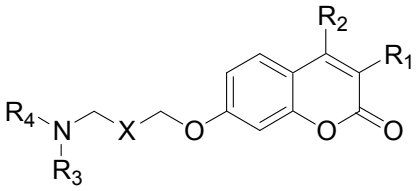

compd	X	R_1	R_2	R_3	R_4	IC_{50}, μM (or inhibition % at 10 μM)			
						MAO-A[a]	MAO-B[a]	AChE[b]	BChE[c]
13		H	H	Me	Me	10	3.2	(38%)	5.3
14[d]		H	H	Et	Et	(43%)	(35%)	1.7	6.8
15		H	H	Me	Bn	(8%)	2.0	2.3	1.0
16[d]		H	H	Me	3-CNBn	(2%)	3.7	4.2	2.8
17[d]		H	H	Me	3-MeOBn	(14%)	2.5	6.6	0.88
18[d]		H	H	Me	3-ClBn	(17%)	3.4	5.7	0.31
19		H	H	Me	Me	(17%)	3.7	7.1	0.24
20		H	H	Et	Et	(9%)	(44%)	2.9	3.4
21		H	H	Me	Bn	(7%)	0.85	0.75	11
22[d]		Me	H	Me	Bn	(0%)	2.4	0.26	1.1
23[d]		H	Me	Me	Bn	(10%)	4.1	0.18	1.0
24[d]		Me	Me	Me	Bn	(0%)	1.2	0.10	0.69
25[d]		H	H	Me	3-CNBn	(5%)	2.8	7.4	4.1
26[d]		H	H	Me	3-MeOBn	(20%)	2.9	4.6	1.4
27[d]		H	H	Me	3-ClBn	(12%)	2.7	0.59	1.2
28[d]		Me	H	Me	3-ClBn	(0%)	4.5	1.3	(29%)
29[d]		H	Me	Me	3-ClBn	(0%)	5.0	0.12	(47%)
30[d]		Me	Me	Me	3-ClBn	(7%)	3.4	0.66	(48%)
31[d]		H	H	Me	4-CNBn	(6%)	0.27	5.6	4.4

32[d]		Me	H	Me	4-CNBn	(15%)	1.7	7.0	(16%)
33[d]		H	Me	Me	4-CNBn	(10%)	0.41	3.3	(29%)
34[d]		Me	Me	Me	4-CNBn	(0%)	2.9	4.2	(18%)
35[d]		CN	H	Me	Bn	(0%)	(41%)	0.20	5.5
36[d]		CN	H	Me	4-CNBn	(0%)	0.99	(42%)	(14%)
37[d]		H	CH_2OH	Me	Bn	(0%)	0.41	0.42	1.1
38		H	CH_2OH	H	Bn	(19%)	0.53	0.44	0.57
39[d]		H	CH_2OH	Me	3-ClBn	(0%)	0.24	0.25	0.63
40[d]		H	CH_2OH	Me	4-CNBn	(0%)	0.035	6.3	(23%)

[a-d] See footnotes of Table 1.

Table 3. Inhibition data of derivatives **42**, **43**, **45**.

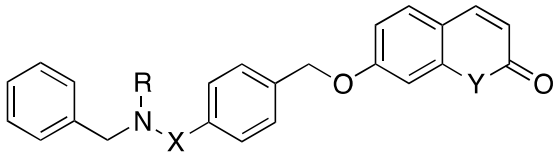

compd	R	X	Y	IC_{50}, μM (or inhibition % at 10 μM)			
				MAO-A[a]	MAO-B[a]	AChE[b]	BChE[c]
42[d]	Me	$-(CH_2)_2-$	O	(12%)	4.1	0.85	0.52
43[d]	H	$-(CH_2)_2-$	O	1.7	(45%)	4.7	0.64
45[d]	Me	$-CH_2-$	NH	(10%)	(29%)	0.49	1.7

[a-d] See footnotes of Table 1.

Table 4. Inhibition data on hMAOs, hAChE and hBChE

compd	IC_{50}, μM (or inhibition % at 10 μM) ± SEM			
	hMAO-A[a]	hMAO-B[a]	hAChE[b]	hBChE[c]
2[d]	(17 ± 6%)	0.134 ± 0.018	1.0 ± 0.1	nt
4	0.48 ± 0.04	0.096 ± 0.006	0.79 ± 0.01	nt
5[d]	0.39 ± 0.05	0.029 ± 0.006	0.30 ± 0.01	0.95 ± 0.02
11	0.191 ± 0.053	0.321 ± 0.038	0.34 ± 0.03	0.95 ± 0.05
12[d]	0.115 ± 0.015	0.018 ± 0.003	0.44 ± 0.06	nt
21	(0%)	0.041 ± 0.008	0.95 ± 0.08	0.89 ± 0.03
22[d]	nt	nt	0.50 ± 0.03	nt
23[d]	nt	nt	0.91 ± 0.07	nt
24[d]	4.3 ± 0.1	0.053 ± 0.001	0.45 ± 0.03	(46 ± 4%)
29[d]	nt	nt	1.0 ± 0.2	nt
31[d]	(0%)	0.045 ± 0.013	6.0 ± 0.5	nt
32[d]	(11 ± 3%)	0.017 ± 0.004	nt	nt
33[d]	(39 ± 2%)	0.039 ± 0.001	8.5 ± 0.8	nt
34[d]	(31 ± 4%)	0.024 ± 0.003	3.9 ± 0.5	nt
37[d]	15.8 ± 2	0.010 ± 0.002	0.12 ± 0.01	9.3 ± 0.7
39[d]	13.0 ± 2	0.024 ± 0.004	0.33 ± 0.03	(14 ± 3%)
40[d]	4.48 ± 0.4	0.0057 ± 0.0008	nt	nt
45[d]	(14 ± 3%)[e]	4.5 ± 0.2	1.5 ± 0.1	nt
Donepezil	(0%)	(0%)	0.015 ± 0.003	4.8 ± 0.6
Clorgyline	0.0049	11.0	nt	nt
Pargyline	4.10	0.13	nt	nt

[a] Human recombinant MAOs on Supersomes™. [b] Human recombinant AChE. [c] Human serum BChE. [d] Hydrochloride salt. [e] Determined at 4 μM concentration. nt, not tested.

Table 5. Bi-directional transport across MDCKII-MDR1 cells of compound **37**.

compd	P_{app}, AP-BL (cm/sec)	P_{app}, BL-AP (cm/sec)	ER[a] P_{app}BL-AP/P_{app}AP-BL
37	$1.91*10^{-5}$	$3.38*10^{-5}$	1.77
Diazepam	$1.56*10^{-5}$	$1.23*10^{-5}$	0.79
FD-4	$1.13*10^{-6}$	$2.68*10^{-7}$	0.23

[a] Efflux ratio (ER) was calculated using the following equation: ER = P_{app}, BL-AP / P_{app}, AP-BL, where P_{app}, BL-AP is the apparent permeability of basal-to-apical transport, and P_{app}, AP-BL is the apparent permeability of apical-to-basal transport. An efflux ratio greater than 2 indicates that a test compound is likely to be a substrate for P-gp transport.

Table 6. Analytical data of compounds **2-40**, **42**, **43**, **45**.

compd	melting point, °C (CC or cryst. solvent)[a]	Analytical calculated %			Analytical found %		
		C	H	N	C	H	N
2[b]	201-3 (CC)	68.12	6.76	3.61	68.10	6.86	3.73
3[b]	183-5 (CC)	68.73	7.02	3.48	68.43	6.75	3.28
4	38-9 (CC)	75.59	7.45	3.83	75.78	7.55	3.61
5[b]	238-40 (CC)	68.73	7.02	3.48	68.40	6.87	3.58
6	66-7 (CC)	75.96	7.70	3.69	75.58	7.45	3.80
7[b]	247-9 (CC)	68.09	6.63	6.35	67.73	6.62	6.09
8[b]	204-6 (CC)	64.00	6.49	3.11	63.94	6.35	2.98
9[b]	201-3 (CC)	68.09	6.63	6.35	67.70	6.53	6.37
10[b]	193-4 (CC)	69.83	7.50	3.26	69.55	7.37	3.31
11	54-5 (CC)	76.30	7.94	3.56	75.99	7.88	3.70
12[b]	171-3 (CC)	70.33	7.72	3.15	70.51	8.03	3.48
13	181-2 (EtOH)	73.77	6.19	4.53	73.42	6.36	4.24
14[b]	225-7 (EtOH)	67.46	6.47	3.75	67.27	6.50	3.79
15	156-7 (CC)	71.67	6.01	3.63	71.29	5.78	3.31
16[b]	132-4 (EtOH)	69.87	5.19	6.27	69.51	5.54	6.03
17[b]	121-3 (EtOH)	69.10	5.80	3.10	68.81	5.64	3.31
18[b]	131-3 (EtOH)	65.80	5.08	3.07	65.55	5.29	3.31
19	108-9 (EtOH/Et_2O)	73.77	6.19	4.53	73.88	6.41	4.35
20	167-8 (EtOH/Et_2O)	74.75	6.87	4.15	74.93	6.47	4.01
21	106-7 (EtOH)	71.67	6.01	3.63	71.44	5.89	3.55
22[b]	> 250 (CC)	71.63	6.01	3.21	71.31	5.95	3.26
23[b]	> 250 (CC)	71.63	6.01	3.21	71.37	6.06	3.34
24[b]	226-8 (CC)	72.07	6.27	3.11	71.77	6.23	3.14

25[b]	129-31 dec (EtOH)	69.87	5.19	6.27	69.64	5.33	6.40
26[b]	128-30 (EtOH)	69.10	5.80	3.10	69.34	5.51	3.23
27[b]	124-6 (CC)	65.80	5.08	3.07	65.97	5.35	3.19
28[b]	> 250 (CC)	66.39	5.36	2.98	66.04	5.29	2.80
29[b]	247-50 dec (CC)	66.39	5.36	2.98	65.99	5.39	2.80
30[b]	236-8 (CC)	66.95	5.62	2.89	67.31	5.80	3.22
31[b]	147-9 (CC)	69.87	5.19	6.27	70.12	5.29	6.37
32[b]	242-4 (CC)	70.35	5.47	6.08	69.99	5.49	6.10
33[b]	224-6 (CC)	70.35	5.47	6.08	70.72	5.59	6.12
34[b]	225-7 (CC)	70.80	5.73	5.90	70.55	5.97	5.76
35[b]	155-7 dec (CC)	69.87	5.19	6.27	69.46	5.55	5.92
36[b]	183-5 dec (CC)	68.72	4.70	8.90	68.88	4.79	8.59
37[b]	235-6 dec (CC)	69.10	5.80	3.10	69.15	5.71	3.43
38	109 dec, 130-2 (EtOH)	74.80	5.77	3.49	74.44	5.69	3.47
39[b]	231-36 (CC)	64.20	5.18	2.88	63.80	5.13	2.89
40[b]	150-2 (CC)	67.99	5.28	5.87	67.61	5.29	5.56
42[b]	207-9 (CC)	71.63	6.01	3.21	71.81	5.91	3.01
43[b]	> 250 (CC)	71.17	5.73	3.32	71.27	5.47	3.37
45[b]	154-5[c] (CC)	71.33	5.99	6.65	71.61	6.04	6.32

[a] CC: column chromatography (see Supporting Information for details). [b] Hydrochloride salt. [c] Free base.

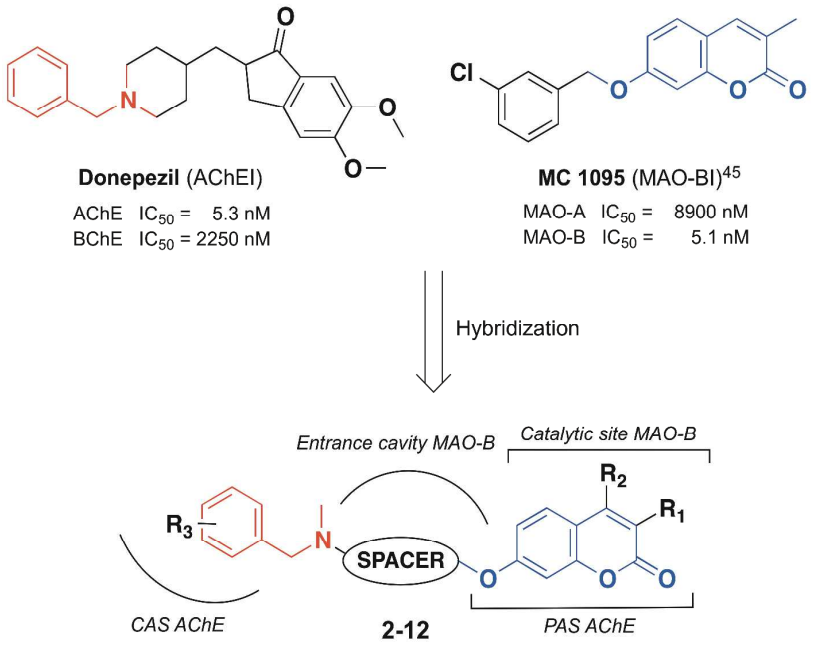

Figure 1. Hybridization strategy for flexible multitarget MAO-B/AChE inhibitors **2-12**.

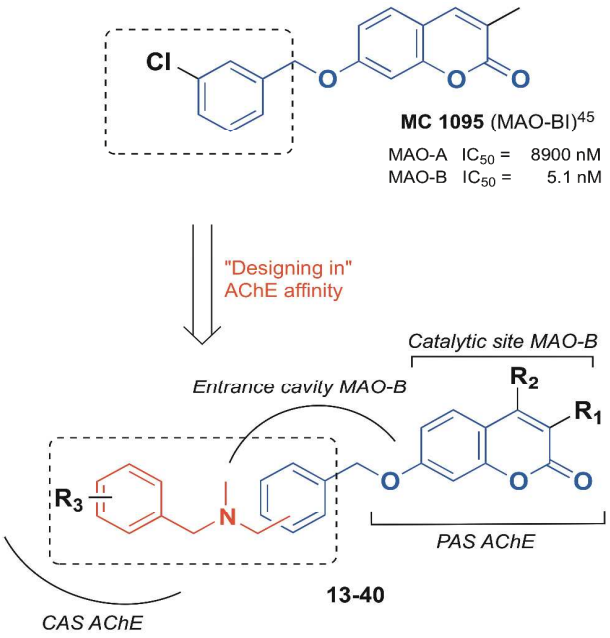

Figure 2. Hybridization strategy for rigid molecules as multitarget MAO-B/AChE inhibitors **13-40**.

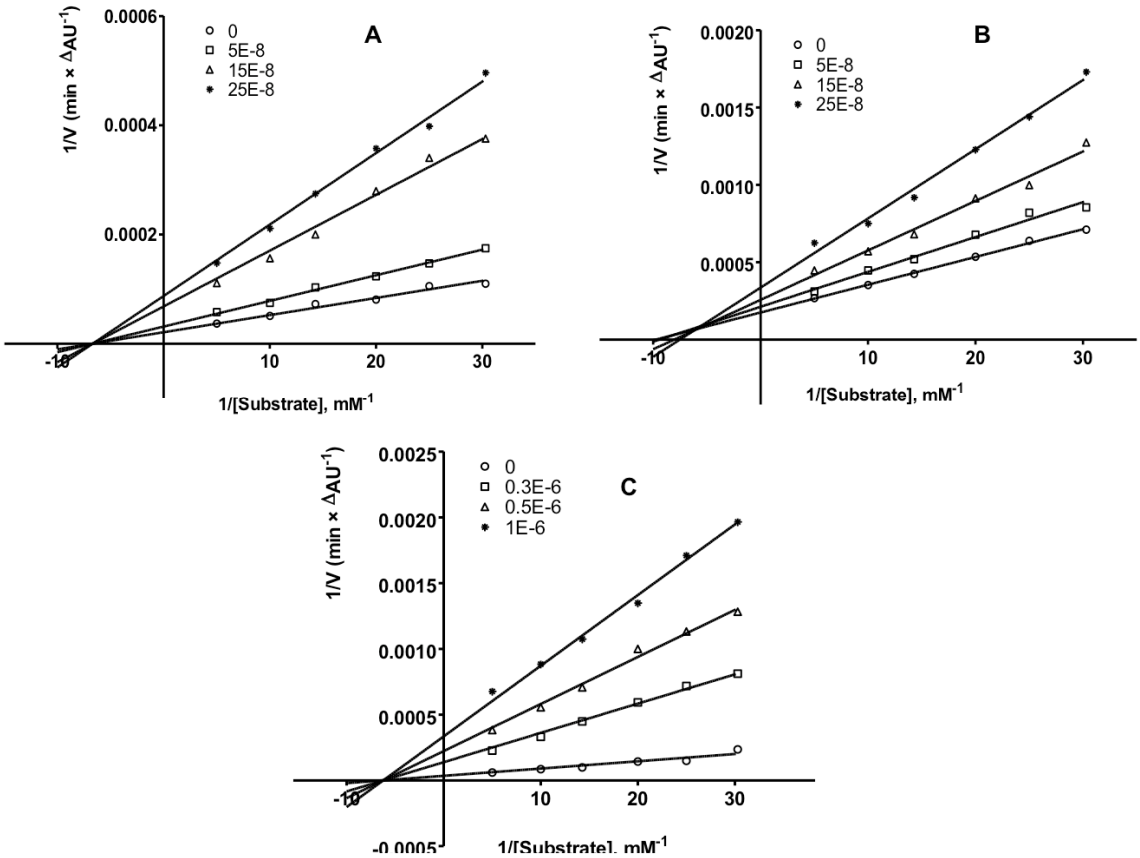

Figure 3. Lineweaver-Burk plots of inhibition kinetics of compounds **11** (A), **24** (B), and **37** (C). Reciprocals of enzyme activity (eeAChE) *vs.* reciprocals of substrate (S-acetylthiocholine) concentration in the presence of different concentrations (0-250 nM) of inhibitor. Concentrations used for inhibitors are reported in inserts.

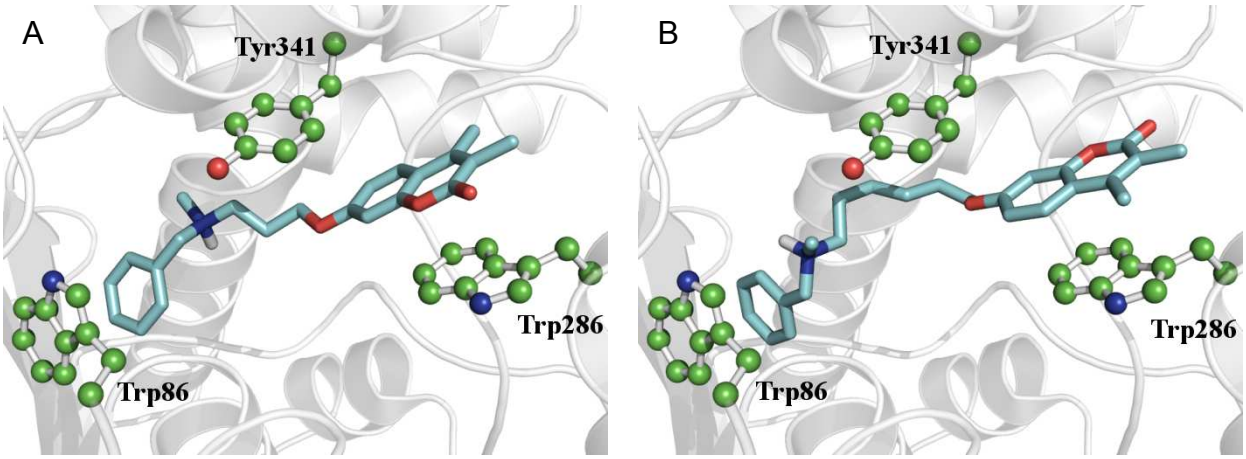

Figure 4. Docking poses of inhibitor **2** (A) and **11** (B) into human AChE binding site (PDB code: 4EY7). Inhibitors are represented in stick while relevant amino acid residues in ball-and-stick, colored according to the atom code (C atoms in cyan an green for inhibitors and amino acid residues, respectively). Docking scores are equal to -98.2 kJ/mol and -106.2 kJ/mol for inhibitor **2** and **11**, respectively.

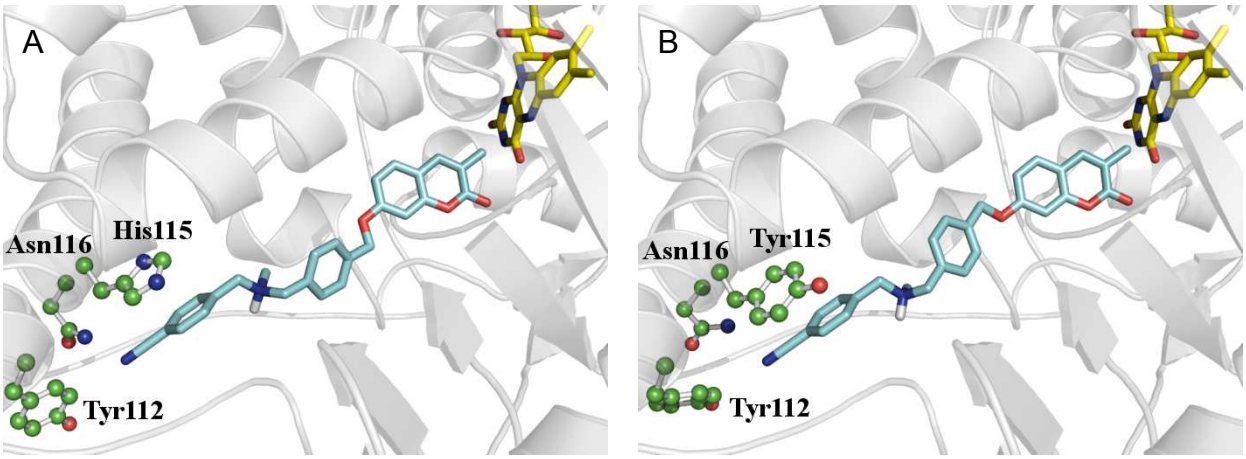

Figure 5. Docking poses of inhibitor **32** into human (PDB code: 2V60) (A) and rat MAO-B (homology model) (B) binding sites. Inhibitors and FAD cofactor are represented in stick while relevant amino acid residues in ball-and-stick, colored according to the atom code (C atoms in cyan, yellow and green for inhibitors, cofactor and amino acid residues, respectively). Docking scores are equal to -88.21 and -80.22 kJ/mol for inhibitor **32** into human and rat isoforms, respectively.

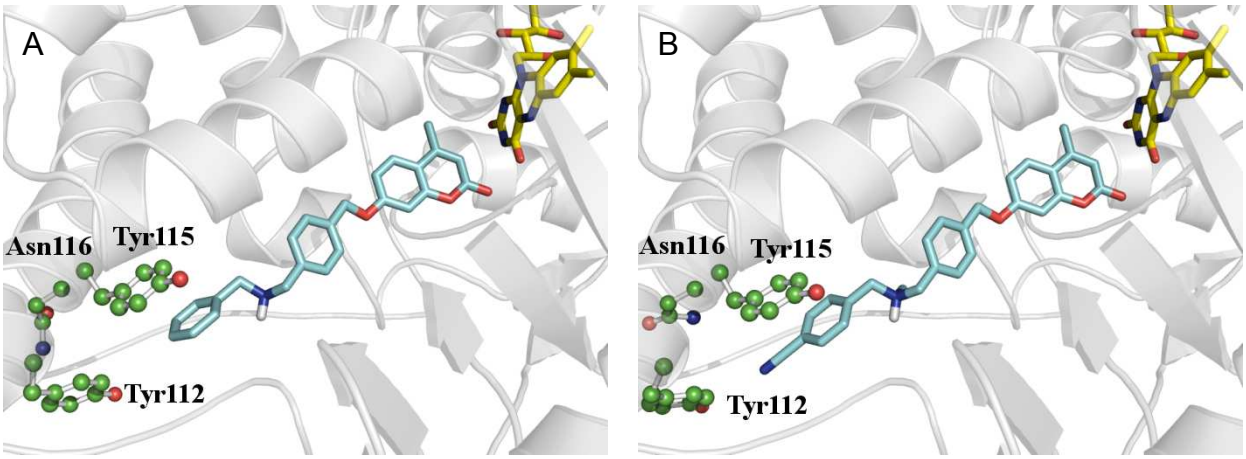

Figure 6. Docking poses of inhibitor **23** (A) and **33** (B) into rat MAO-B binding site (homology model). Inhibitors and FAD cofactor are represented in stick while relevant amino acid residues in ball-and-stick, colored according to the atom code (C atoms in cyan, yellow and green for inhibitors, cofactor and amino acid residues, respectively).

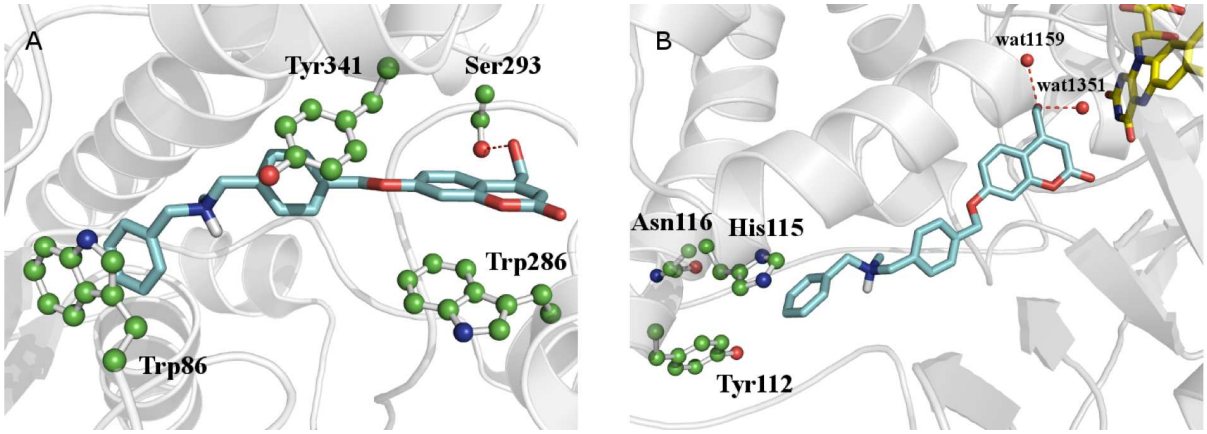

Figure 7. Docking poses of inhibitor **37** into (A) hAChE (PDB code: 4EY7) and (B) hMAO-B (PDB code: 2V60) binding sites. Inhibitors are represented in stick while relevant amino acid residues in ball-and-stick, colored according to the atom code (C atoms in cyan an green for inhibitors and amino acid residues, respectively). Structural water molecules (that are HOH1159 and HOH1351 according to the numbering of 2V60) are represented as red balls. Hydrogen bonds are represented as red dashed lines. Docking scores are equal to -109.38 kJ/mol and -95.95 kJ/mol for inhibitor **37** into hAChE and hMAO-B, respectively.

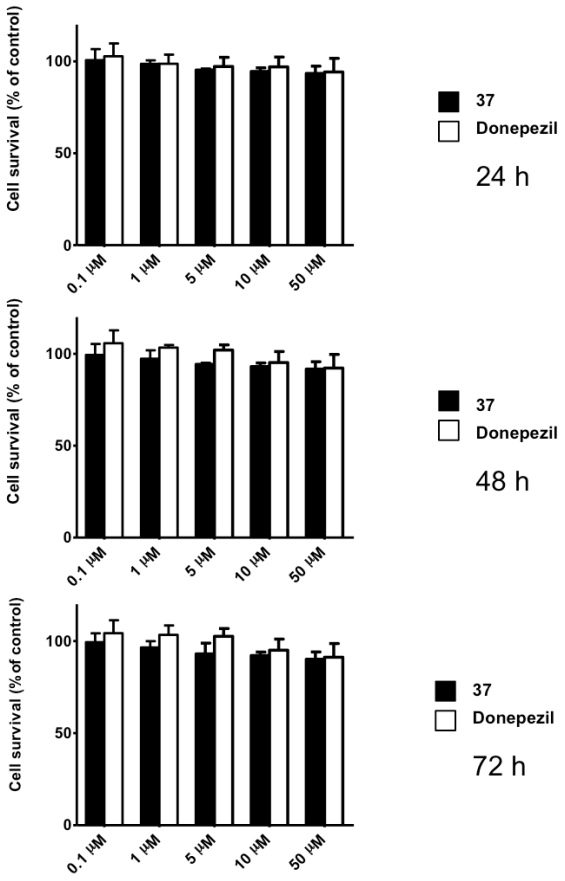

Figure 8. Viability of human neuroblastoma SH-SY5Y cells exposed to compound **37** at different concentrations and incubation times. SH-SY5Y cells were incubated with increasing concentrations (range 0.1–50 μM) of the test compounds for 24, 48 and 72 h. Untreated cells were used as control. Results are expressed as percentage of viable cells observed after treatment with compounds **37** and donepezil vs. untreated control cells (100%) and shown as mean ± SD (n = 3).

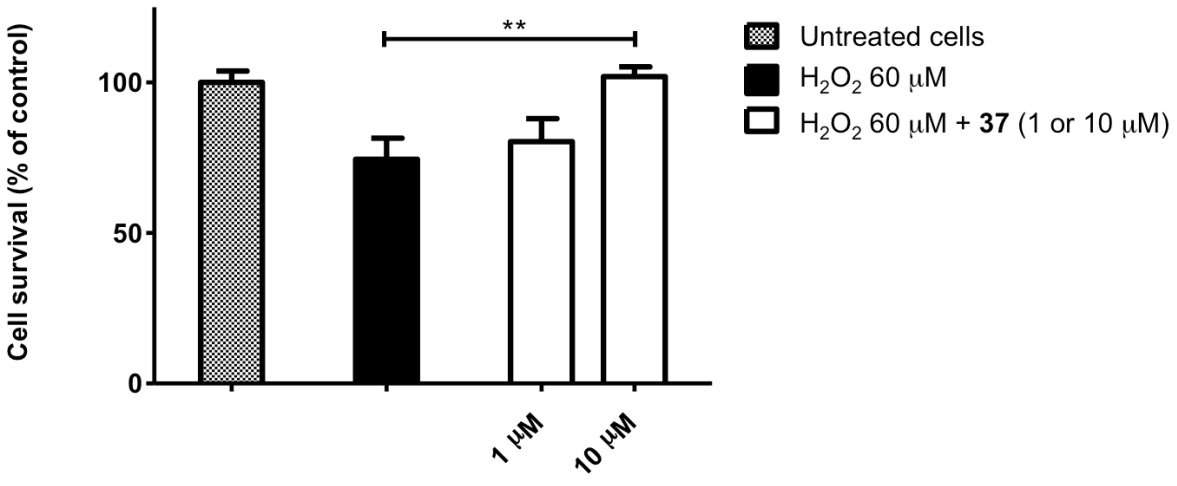

Figure 9. Percentage of cell survival in the human neuroblastoma cell line SH-SY5Y of compounds **37** in the following conditions: untreated cells (grey column), in the presence of H_2O_2 (60 μM) alone (black column), in the presence of both H_2O_2 (60 μM) and compound **37** (1 and 10 μM, white columns). Data represent means ± SD (n = 3); statistical significance was estimated using one-way ANOVA and Bonferroni post hoc test (** $P < 0.01$).

Table of contents graphic

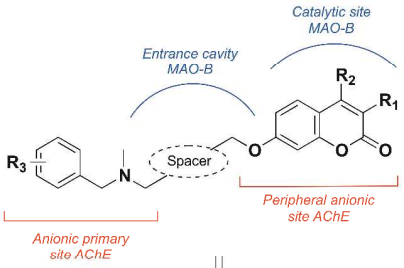

MTDL:
Dual AChE-MAO B Inhibitors

	IC_{50} (μM)			
	hMAO-A	**hMAO-B**	**hAChE**	
Cp. 37	15.8	0.010	0.12	BBB-permeant, neuroprotective, not cytotoxic, poor P-gp substrate